TECTONICS, VOL. 1, NO. 1, PAGES 21-56, FEBRUARY 1982

TECTONICS AND TOPOGRAPHY FOR A LITHOSPHERE CONTAINING DENSITY HETEROGENEITIES

Luce FLEITOUT and Claude FROIDEVAUX

Laboratoire de Géophysique et Géodynamique interne
Université Paris-Sud, 91405 ORSAY, France.

Abstract. The purpose of this paper is to clarify the dynamic role of lithospheric density heterogeneities, in particular with respect to mountain building and other processes of intraplate deformation. Density anomalies within or just beneath the lithosphere constitute major sources for tectonic stress fields : the product of their magnitude by their depth is shown to characterize their ability to induce deformation. This rule of the density moment directly yields the lithospheric thickening or thinning rate when applied to structures of large lateral extent. For anomalies of lateral extent that is small in comparison with their depth, the deformation is vertically inhomogeneous and has been computed with the help of simple physical models of a stratified viscous Newtonian lithosphere. The analytical treatment is based on Fourier transform. Continent-continent collision thickens not only the crust but the entire lithosphere. The cold root underlying a mountain chain induces strong regional compressive stresses able to sustain the mountain bulding process without further help from forces transmitted from far away. Thus the continental lithosphere is in a somewhat metastable mechanical state. Adiabatic, i.e. rapid, thickening (or thinning) tends to grow further once initiated. Tectonic phases of strong compression correspond to the climax of such instabilities. The response of models with cold lithospheric roots of various intensities has been computed both in two and three dimensions. They yield velocity distributions and stress fields. Instructive comparisons are made with earthquake focal mechanisms and in situ stress measurements in the Alpine and Appalachian regions. In the presence of lateral variations of the mechanical properties of the lithosphere, the tectonic style is not only function of the local topography and of the nature of its compensation. Deformations in neighbouring provinces are coupled as shown by 3-dimensional models. For example, thickening sustained by a cold lithospheric root may generate extension in peripheral zones of weakness. These last results illustrate the point that the computation of regional tectonic stresses requires the knowledge of the density anomalies within the lithosphere on the one hand, and of geometrical constraints related to lateral mechanical heterogeneities on the other.

1. INTRODUCTION

Stresses within the lithosphere are sensitive to the global dynamics of the plates. Thus attempts have been made to model these stresses by applying appropriate forces at the plate boundaries [Richardson et al., 1979]. Such models based on homogeneous plates cannot account for abrupt changes in the stress patterns observed in certain regions. For instance, the compressional direction in the Alpine region determined by earthquake focal mechanisms remains perpendicular to the mountain chain at the bend

Paper number 1T1780. 0278-7407/82/001T-1780$10.00

between the central and the western Alps [Pavoni, 1977 ; Fréchet, 1978 ; Philip, 1980]. In the Appalachians and in the Colorado plateau, in situ measurements display stress azimuths orthogonal to those of surrounding regions [Zoback and Zoback, 1980]. Another case is the Aegean basin where extension changes to compression along the western and southern edges of the region [Le Pichon and Angelier, 1979 ; Mercier, 1981 ; McKenzie, 1978 ; Paquin et al., 1982]. One way out is to invoke possible lateral mechanical heterogeneities within the plate. Indeed the presence of zones of weakness or, on the contrary, of hard cores can generate local variations in the tectonic style [Tapponnier and Molnar, 1976 ; Tapponnier, 1977].

The other alternative, which will be emphasized in this paper, is to take account of local sources for the lithospheric stress field. These sources are caused by lateral variations in the density distribution of thermal or lithological origin. For instance, it has been demonstrated that topography and its compensation at depth can generate sizable stresses capable of influencing the tectonic style [Frank, 1972 ; Artyushkov, 1973]. A good illustration is that the mass defect in the mantle under ridges and rifts is responsible for both the regional elevated topography and the extensional regime of those structures. This last example should not yield the impression that a straightforward correlation between topography and stress-style always holds. On the contrary other elevated regions can suffer stronger compression than their surroundings: this is the case for most collisional mountain chains. Similarly, but on a larger scale, continents, which are more elevated than oceanic ridges, are often in compression.

The main purpose of this paper is to clarify the relationship between lateral density variations in the lithosphere and observed topography and stress field. The first section is a general study of the physical mechanisms. It defines the properties of the model lithosphere and the applied boundary conditions. A simple two layer model is solved analytically and provides adequate physical insight as to the influence of the depth and wavelength of the mass variations upon the induced topography and surface stresses. A more elaborate set of models includes more realistic distributions of mass heterogeneities and mechanical properties. Some of these considerations are put in appendices so that only the most important conclusions appear in the main text. This presentation was chosen for the sake of readers who would be most interested in the geophysical applications. The latter are found in the next parts of the paper. Section 3 considers cases treated in two dimensions with strong emphasis given to the role of lithospheric thickening in the moutain building process. It is usually assumed that forces responsible for the deformation in a collision region are transmitted through the adjacent lithospheric plates. We shall show that the mechanical instability, which exists once a lithospheric cold root has been created, is capable by itself of sustaining the compressional tectonics. The existence of a cold lithospheric root is well demonstrated by the seismic data in the Central Alps [Sprecher, 1976 ; Panza and Mueller, 1979 ; Baer, 1980 ; Hovland et al., 1981 ; Werner and Kissling, 1981]. Section 4 attempts to explore possible limitations of the two-dimensional treatments by extending this study to three dimensions. It should provide a good basis for the modelling of regional intraplate deformation and stress fields. It analyzes the importance of geometrical factors related to lateral variations of density and mechanical heterogeneities. A possible novelty is the contingent presence of zones of extension in the foreland of mountain massifs.

2. THE BASIC PHYSICAL MODEL

The Earth's lithosphere exhibits a rich variety of mechanical behaviors. On the global scale of plate tectonics it may be pictured as rigid. However intraplate deformation phenomena are known to occur at all scales.

As the case may be, lithospheric deformations can be brittle, elastic, or viscous. Here we shall consider a model lithosphere composed of several layers of uniform Newtonian viscosity, underlain by a viscous asthenosphere and possibly overlain by an elastic lid. This simplification has the great advantage of allowing to treat the problem analytically while retaining the main physical implications. First we will also assume the problem to be two-dimensional. Mass heterogeneities are either concentrated between two layers or spread uniformly over the whole depth of a given layer. Their variation in one horizontal direction, x, can be split into components of various wavelengths (Fourier transform). It is then simple to study the effect of a simple harmonic, i.e. of a sinusoidal mass fluctuation :

$$\Delta\rho = \delta\rho \cos(kx) \qquad (1)$$

where k the wavenumber equals $2\pi/\lambda$, λ being the wavelength.

The lateral mass variation induces a flow in the whole structure. The resulting surface stresses and deformations can thus be predicted. In particular, the induced topography and superficial tectonic regime will be discussed in some detail. More precisely the quantification of this problem derives from the solution of the Navier-Stokes equations, relating velocity changes to driving forces, combined with the mass conservation or continuity equation (see appendix 1). These solutions are, of course, functions of the applied boundary conditions : at the surface

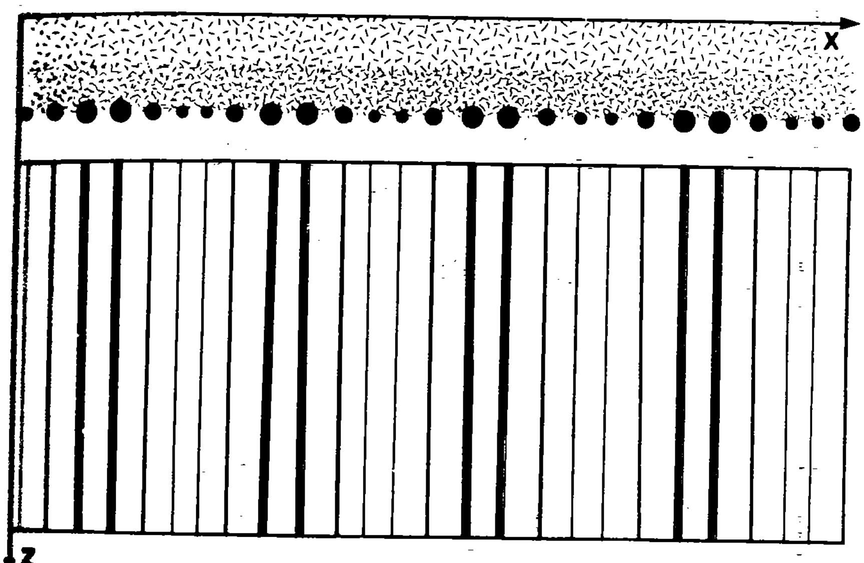

Fig. 1. Lithospheric model consisting of five viscous layers and including sinusoidal mass heterogeneities. Layers 1 and 2 represent the crust. They have the same nondimensional width (0.2) and viscosity ($10\eta_o$) as layer 3, which belongs to the mantle lithosphere. The mass heterogeneity called ∂m in the text and marked by black beads in the figure is located at the interface between the crust and the mantle. Layer 4 also belongs to the lithosphere. It has a viscosity η_o, a nondimensional thickness 1.5 and contains density heterogeneities depicted by vertical lines of varying thickness. Layer 5 is equally made of mantle material. It extends to infinity and has a viscosity ($\eta_o/100$). The viscosities mentioned here are those of our standard model. Other sets of values are also considered in the text.

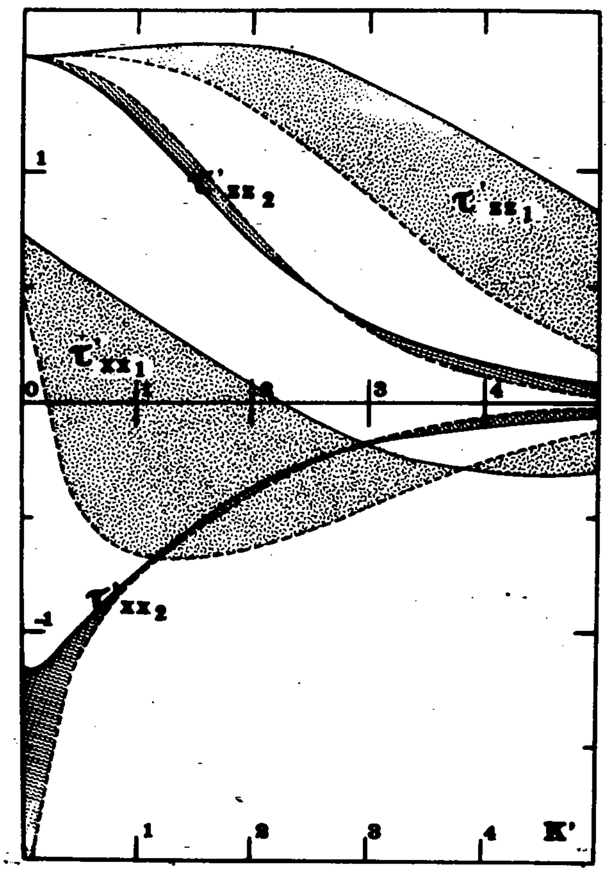

Fig. 2. Stresses and horizontal velocity gradients at zero depth versus wavenumber k' characterizing the spatial variation of the mass anomalies. Indices 1, resp. 2 refer to mass heterogeneities at the Moho, resp. density heterogeneities in the lower lithosphere. Full lines give solutions for the standard viscosity distribution. Dashed lines are for a similar set of viscosity values except that of layer 2, which has been reduced to $0.1\eta_0$. The shaded area indicates the difference between the solutions for these two viscosity distributions. The various quantities are nondimensional. They correspond to a mass fluctuation of amplitude 1.5 at the Moho or to a density variation of amplitude 1 in the lower lithosphere. The relationship between nondimensional quantities is given by (A17). Thus for a characteristic length ℓ_0 = 100 km, k' = 1 corresponds to k = 10^{-5} m^{-1} and therefore to a wavelength $\lambda = 2\pi/k$ amounting to 628 km. For the stresses, the dimensional value is readily found, if one notices that for k = 0 the local compensation implies a vertical stress equal to the weight of the underlying mass anomalies.

two quantities must vanish. One is the vertical velocity. The other depends upon the absence or existence of the elastic lid. In the first case the shear stress is zero at the surface (free slip). The computed solutions yield the vertical normal stress, from which one evaluates the topography, as well as the horizontal velocity gradient, which one may compare to the tectonic deformation. In the second case the computed vertical stress plays a similar role, but the surface velocity in the fluid vanishes. The relevant quantity is the surface shear stress in the viscous fluid which is operative in inducing horizontal compression or extension in the lid. The reader is refered to the appendices for a full

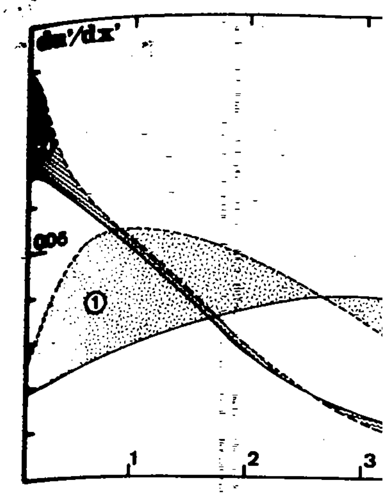

Fig. 2. (continued)

mathematical treatment, and t
A certain number of simple
cally (appendix 2). The corre
teristics, also found in more
wavelengths the computed surf
the mass variation at depth.
sustained topography. This do
rison with the depth of the d
then attenuated. In the prese
also show that, at large wave
stresses within the lid is pr
riation.
In order to simulate a sit
let us consider a structure c
The first two correspond to t
phere, and the lower one to a
thicknesses are given in a no
by 75 or 100 km to correspond
starting point we take a basi
layers 1, 2, and 3, η_0 for la
hereafter referred to as the s
the above viscosity contrasts
models. In particular, the cas
will be found instructive. Fig
terogeneities. One is concentr
and simulates the effect of Mo
tributed in layer 4 and reflec
within the lower lithosphere.
proceeds as in appendix 2. The
which makes a total of 20 in t
by matrix inversion.
Figure 2 depicts the variat
stresses and of the horizontal
wave number. Four curves are g
spond to the standard set of v
correspond to the same structu
by a factor of 100. Density va
lower lithosphere (index 2) ar
solutions will be analyzed sho
of the vertical stress for sho

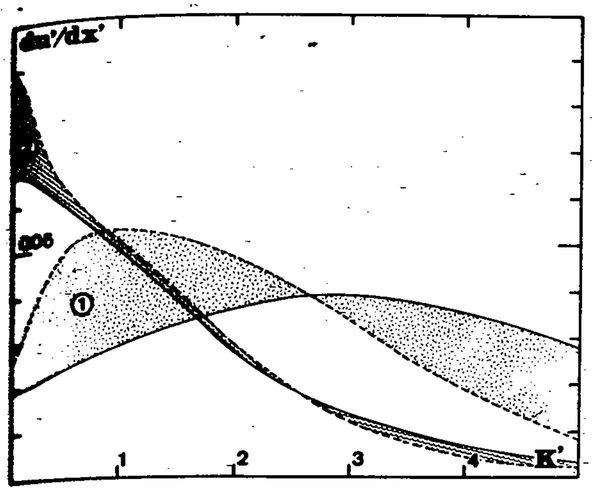

Fig. 2. (continued)

mathematical treatment, and the definition of non-dimensional variables.

A certain number of simple structures can readily be handled analytically (appendix 2). The corresponding solutions bear interesting characteristics, also found in more elaborate models presented below. At large wavelengths the computed surface vertical stress equals the weight of the mass variation at depth. This implies a perfect compensation of the sustained topography. This does not hold at wavelengths short in comparison with the depth of the density anomaly : the induced topography is then attenuated. In the presence of a lid the simple analytical models also show that, at large wavelengths the intensity of the horizontal stresses within the lid is proportional to the depth of the density variation.

In order to simulate a situation somewhat comparable to the real Earth, let us consider a structure consisting of five layers as in Figure 1. The first two correspond to the crust, the next two to the mantle lithosphere, and the lower one to an astenosphere extending to infinity. The thicknesses are given in a non-dimensional form and can be multiplied by 75 or 100 km to correspond to standard dimensions (appendix 1). As a starting point we take a basic set of viscosities equal to $10\eta_o$ for layers 1, 2, and 3, η_o for layer 4 and $0.01\eta_o$ for layer 5. This model is hereafter referred to as the standard lithospheric model. Departures from the above viscosity contrasts will help testing the sensitivity of the models. In particular, the case of a lower crust with a reduced viscosity will be found instructive. Figure 1 also shows two kinds of density heterogeneities. One is concentrated at the interface between two layers and simulates the effect of Moho undulations. The other is uniformly distributed in layer 4 and reflects compositional or thermal mass variations within the lower lithosphere. For this five layer model the computation proceeds as in appendix 2. There are four integration constants per layer, which makes a total of 20 in this model. They are obtained numerically by matrix inversion.

Figure 2 depicts the variation of the surface value of the two normal stresses and of the horizontal velocity gradient as a function of the wave number. Four curves are given for each quantity : full curves correspond to the standard set of viscosities of Figure 1, dashed curves correspond to the same structure but with a lower crust viscosity reduced by a factor of 100. Density variations at the Moho (index 1) and in the lower lithosphere (index 2) are considered. Various aspects of these solutions will be analyzed shortly. One is the already mentionned fall of the vertical stress for short wavelengths (large k). The variation

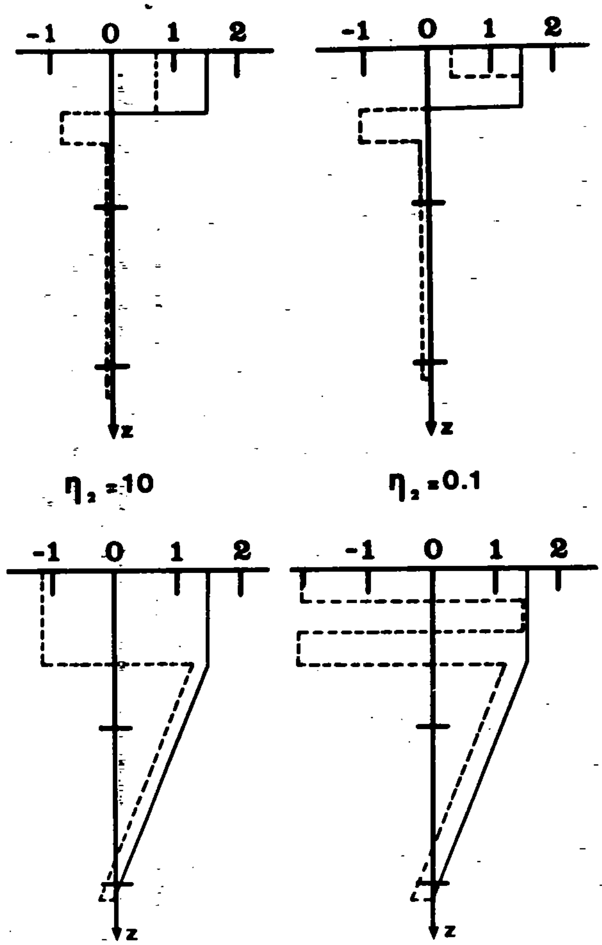

Fig. 3. Vertical stress τ_{zz} (full line) and horizontal stress τ_{xx} (dashed line) versus depth for a small wavenumber k' = 0.05. The four solutions correspond to two types of mass heterogeneities and to two different values of the viscosity in the lower crust. At the top, the model lithosphere constains a mass fluctuation ∂m = 1.5 located at the Moho. At the bottom, the density heterogeneity $\partial\rho$ = 1 is located in the lower lithosphere. The left hand solutions correspond to our standar viscosity model, whereas the right hand ones include a soft lower crust.

with depth of both normal stresses τ_{zz} and τ_{xx} is given in Figure 3 for very long wavelength (k' = 0.05). All four models corresponding to Figure 2 are also shown. Figure 4 depicts the same quantities for the same models but for rather short wavelength (k' = 3). For a crustal thickness of 40 km these two extreme values of k' correspond to lateral variations with wavelengths of 12000, resp. 200 km.

a. Mechanical Behavior for Large Wavelengths: The Rule of the Density Moment

The computed values at large wavelength (k' << 1) can be understood on the basis of simple physical arguments. Let ℓ be the depth limit for density heterogeneities and let the viscosity beyond this depth be sufficiently small for the non hydrostatic vertical stress to be negligible.

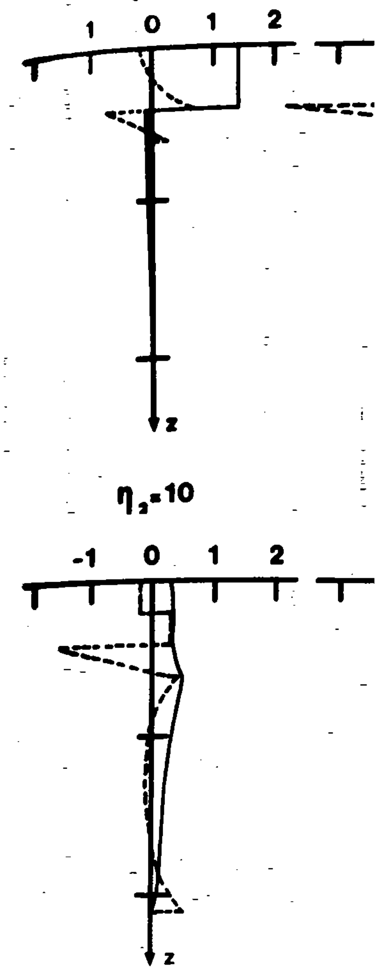

Fig. 4. Similar to Figure 3

Thus τ_{zz} at any depth z_o is e
below this depth :

$$\tau_{zz} = \int_{z_o}^{\ell} \Delta\rho g dz$$

where g stands for the gravit
tical equilibrium equation :

$$\frac{\partial\tau_{zz}}{\partial z} = \frac{-\partial\tau_{xz}}{\partial x} + \Delta\rho g \simeq \Delta\rho$$

as $\partial\tau_{xz}/\partial x = k\tau_{xz}$ becomes ne
illustrated by the solutions
finite value at the depth of
centrated (top part of the fi
lithosphere containing the h
figure).

The tendency of the litho
difference between the norma
spheric thickness. Let us fi
single density fluctuation Δ
stress τ_{zz} vanishes below z

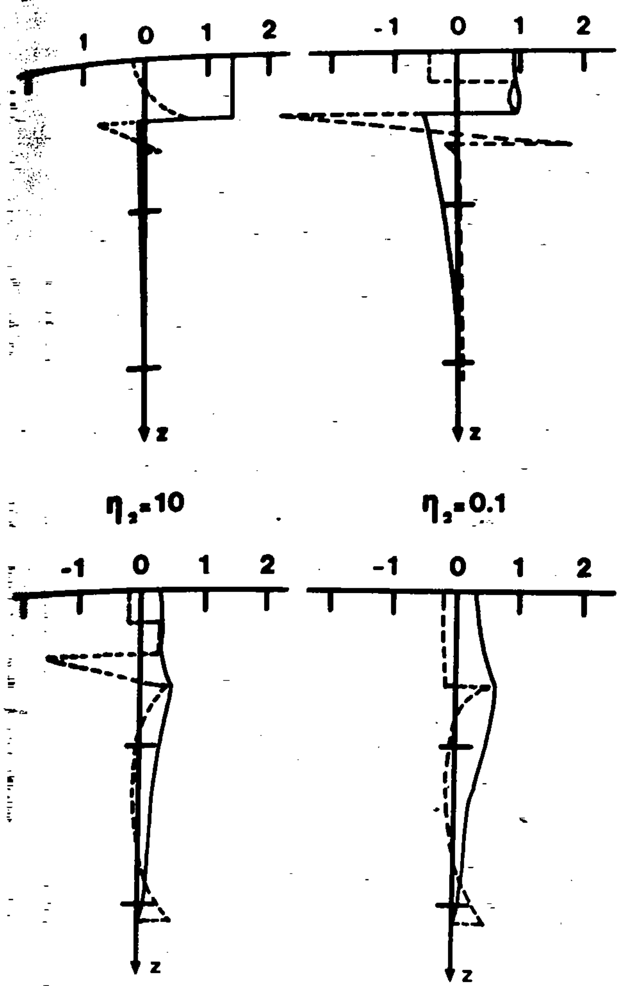

Fig. 4. Similar to Figure 3 but for a large wavenumber k' = 3.

Thus τ_{zz} at any depth z_o is equal to the weight of the density anomalies below this depth :

$$\tau_{zz} = \int_{z_o}^{\ell} \Delta\rho g dz \qquad (2)$$

where g stands for the gravity acceleration. This derives from the vertical equilibrium equation :

$$\frac{\partial\tau_{zz}}{\partial z} = \frac{-\partial\tau_{xz}}{\partial x} + \Delta\rho g \simeq \Delta\rho g$$

as $\partial\tau_{xz}/\partial x = k\tau_{xz}$ becomes negligible at small k. Equation (2) is well illustrated by the solutions shown in Figure 3. There τ_{zz} jumps to a finite value at the depth of the Moho where the mass variation is concentrated (top part of the figure) or increases linearly within the lower lithosphere containing the homogeneous density anomaly (bottom part of the figure).

The tendency of the lithosphere to vary in thickness is related to the difference between the normal stresses averaged over the entire lithospheric thickness. Let us first compute $\bar{\tau}_{zz}$. We have just seen that for a single density fluctuation $\Delta m = \Delta\rho dz$ located discretely at a depth z, the stress τ_{zz} vanishes below z and equals $\Delta m g$ from z to the surface. The average stress is thus $\Delta mgz/\ell$. Hence for a distributed density fluctuation $\Delta\rho$, one has :

$$\bar{\tau}_{zz} = \frac{g}{\ell}\int_0^{\ell} \Delta\rho z\, dz = \frac{gM}{\ell} \tag{3}$$

where M, given by the above integral, is the moment of the density anomalies with respect to the surface. This physical quantity will play a key role in understanding intraplate dynamics.
Integrating the horizontal equilibrium equation $\partial\tau_{xx}/\partial x + \partial\tau_{xz}/\partial z = 0$ over the lithospheric thickness one finds :

$$\frac{\partial\bar{\tau}_{xx}}{\partial x} = -\frac{\tau_{xz}(\ell)}{\ell} \tag{4}$$

where $\tau_{xz}(\ell)$ is the drag at the base of the lithosphere. The density fluctuations do not contribute to the value of the average horizontal compression τ_{xx}. Focussing the attention to the effect of these fluctuations one sees that the quantity $(\bar{\tau}_{zz} - \bar{\tau}_{xx})$ varies in proportion to the moment M. All of the above is true independently of the particular rheology of the structure. The latter could just as well be elastic or rigid plastic and laterally heterogeneous, the tendency for lithospheric thickening or thinning would always be governed by the magnitude of M, the moment of the mass heterogeneities. This simple rule is similar to that derived for layers of variable thickness [Artyushkov, 1973 ; Dalmayrac and Molnar, 1981].

In the particular case of a viscous lithosphere one has the local equation :

$$\tau_{xx} - \tau_{zz} = 4\eta\frac{\partial u}{\partial x} \tag{5}$$

For large wavelengths the horizontal velocity gradient does not vary with depth (see equation (A12) in appendix 1 which shows a variation in e^{ky} or e^{-ky}). The contribution induced by the mass heterogeneities is therefore:

$$\frac{\partial u}{\partial x} = \frac{\bar{\tau}_{xx} - \bar{\tau}_{zz}}{4\bar{\eta}} = -\frac{Mg}{4\bar{\eta}\ell} \tag{6}$$

This simple formula explains two features in Figure 2. The deeper the density anomaly the larger the moment M. Hence the larger $\partial u/\partial x$ values for case 2 than for case 1 near $k = 0$. In other words a given mass fluctuation induces larger tectonic deformations when located in the lower lithosphere rather than at the Moho. The second feature is the enhancement of $\partial u/\partial x$ by the introduction of a soft lower crust which decreases the mean viscosity.

The depth variation of the horizontal stress τ_{xx} can now be derived from (5) by introducing (2) and (6). The value of the deviatoric stress becomes :

$$\tau_{xx} - \tau_{zz} = -\frac{\eta}{\bar{\eta}}\frac{Mg}{\ell} \tag{7}$$

This expression explains the strong variations of τ_{xx} in Figure 3 (dashed curves) between layers of different viscosity η. Strong deviatoric stresses are concentrated in the most competent layers. The figure also illustrates the fact that $\bar{\tau}_{xx} = 0$.

This last remark can help illustrating the case of a highly viscous lid of thickness d and much smaller viscosity with a mass fluctuation Δm concentrated at the base of the lithosphere. According to (3) the stress τ_{zz} amounts to $g\Delta m$ at all depths. According to (7) $\tau_{xx} = \tau_{zz}$ in the weak

lower layer. To have a global z
top competent layer must satisf

$\tau_{xx} = \frac{-\Delta mgd}{h}$

This is identical to the result
of appendix 2 and showing once r
ger the induced surface horizont
the limit kd << 1.

b. Variation of the Solutions fo

The physical arguments preser
lengths (kd > 1). For instance
ported by horizontal variations
cannot be neglected. Thus equati
graphy does no longer correspond
anomalies. The decrease of τ_{zz} t
the decrease starts at smaller k
Similarly $\partial u/\partial x$ is no longer dep
The vertical profiles of τ_{zz} and
plicity of those described in Fi
wavelengths the tectonic effects
those of deeper sources. To see
curves in Figure 2.

Other models similar to the o
computed in order to assess the
or of a stiffer asthenosphere. T
They do not significantly differ

3. LITHOSPHERIC THICKENING (OR T

Alpine type mountain chains a
this fact could be in contradict
in the previous section. Indeed
graphy to spread is proportional
The latter can often be express
pography by the depth of compens
remove this difficulty is to inv
out the colliding plates capable
ation is then thought to be loca
[Artyushkov, 1974 ; Molnar and Ta
tainly relevant for mountain bui
a mechanism equally capable of ge
of localizing the crustal deforma
of the fact that in continental c
only the crust but the entire lit
below the mountain chain. This ha
Alps on the basis of seismic and
Werner and Kissling, 1981]. The e
known. Like thrusting in the surf
asymmetrical and heterogeneous. S
the fact that the thickening fact
and for the crust. The cold root
it has a tendency to sink. This g
the upper lithosphere. This mecha
plaining the tectonics of northwe
1978]. Here we shall quantify thi
the time evolution will be invest
assumptions. Second, a more preci
cally and the results will be pre

lower layer. To have a global zero average, the horizontal stress in the top competent layer must satisfy the relation :

$$\tau_{xx} = \frac{-\Delta m g d}{h}$$

This is identical to the result obtained with an elastic lid at the end of appendix 2 and showing once more that the deeper the source, the stronger the induced surface horizontal stresses. All this of course within the limit $kd \ll 1$.

b. Variation of the Solutions for Decreasing Wavelengths

The physical arguments presented above are not valid at short wavelengths ($kd > 1$). For instance the density anomaly can be partially supported by horizontal variations of the shear stress : $\partial\tau_{xz}/\partial x \simeq k\tau_{xz}$ cannot be neglected. Thus equation (2) for τ_{zz} does not apply : the topography does no longer correspond to the weight of the underlaying density anomalies. The decrease of τ_{zz} takes place for $kd > 1$. This explains that the decrease starts at smaller k values for deeper sources (figure 2). Similarly $\partial u/\partial x$ is no longer depth independent and (6) does not apply. The vertical profiles of τ_{zz} and τ_{xx} shown in Figure 4 have lost the simplicity of those described in Figure 3. Unlike what was said for large wavelengths the tectonic effects of shallow sources may here dominate those of deeper sources. To see that, observe the crossing of the $\partial u/\partial x$ curves in Figure 2.

Other models similar to the one pictured in Figure 1 have also been computed in order to assess the influence of a stiffer upper lithosphere or of a stiffer asthenosphere. The solutions can be found in appendix 3. They do not significantly differ from those discussed above.

3. LITHOSPHERIC THICKENING (OR THINNING)

Alpine type mountain chains are usually in compression. Apparently this fact could be in contradiction with the major proposal formulated in the previous section. Indeed the predicted tendency of a high topography to spread is proportional to the moment M (equation (6) and (7)). The latter can often be expressed by the product of the mass of the topography by the depth of compensation (see equation (3)). One way to remove this difficulty is to invoke strong compressional stresses throughout the colliding plates capable of sustaining the mountain. The deformation is then thought to be localised in zones of lithospheric weakness [Artyushkov, 1974 ; Molnar and Tapponnier, 1981]. Such arguments are certainly relevant for mountain building processes. Here, however, we propose a mechanism equally capable of generating large compressive stresses and of localizing the crustal deformation. This new approach takes account of the fact that in continental collision the thickening involves not only the crust but the entire lithosphere. A cold root forms at depth below the mountain chain. This has been well documented for the Central Alps on the basis of seismic and gravity data [Panza and Mueller, 1979 ; Werner and Kissling, 1981]. The exact geometry of this cold root is not known. Like thrusting in the surficial geological layers it may well be asymmetrical and heterogeneous. Such details are not essential but for the fact that the thickening factors are identical for the lithosphere and for the crust. The cold root being denser than the surrounding mantle, it has a tendency to sink. This generates local compressive stresses in the upper lithosphere. This mechanism has already been suggested for explaining the tectonics of northwestern Greece and Albania [McKenzie, 1978]. Here we shall quantify this problem in two different ways. First, the time evolution will be investigated on the basis of some simplifying assumptions. Second, a more precise configuration will be treated numerically and the results will be presented in graphical form.

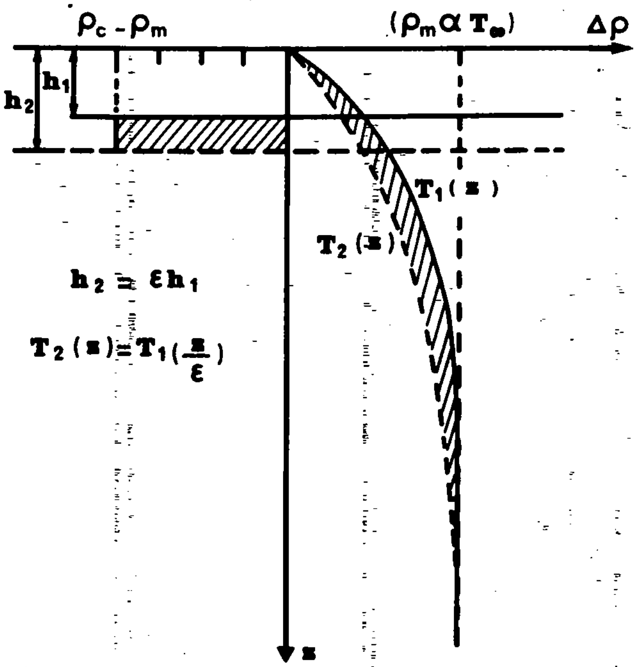

Fig. 5. Density variations, versus depth, following homogeneous lithospheric thickening by a factor ε. The crustal thickness increases from h_1 to h_2. This gives rise to a negative density fluctuation of amplitude $\rho_c - \rho_m$ (where the indices c and m refer to crust and mantle). The location of this density anomaly is defined by the shaded area on the left hand side on the left hand side of the picture. The right hand side pictures the density anomalies (shaded area) related to temperature differences. T_1 is the original profile and T_2 is the new profile after adiabatic thickening. The resulting density anomalies equal $\rho_m \alpha(T_1 - T_2)$, where α is the coefficient of thermal expansion. Notice that the scale for Δρ is not the same on both sides of the picture (the thermally induced heterogeneity is enhanced by about a factor 4).

a. Metastable Continental Lithosphere

Let us consider a simplified lithospheric thickening process where each mass element originally at a depth z is brought adiabatically to the depth εz. The corresponding Moho deflection introduces a mass deficiency that will tend to oppose further lithospheric thickening. The cold root on the other hand represents a mass excess of smaller magnitude but located at greater depth. Whether its destabilizing influence will overcome the stabilizing effect of the crustal root depends upon the sign of the total moment of the two density anomalies.

$$M = -(\rho_m - \rho_c)\int_{h_c}^{\varepsilon h_c} z\,dz + \int_0^{\infty} \alpha\,\rho \left[T_1\left(\frac{z}{\varepsilon}\right) - T_1(z)\right] z\,dz$$

$$= -(\rho_m - \rho_c)\,\frac{h_c^2}{2}\,(\varepsilon^2 - 1) + \int_0^{\infty} \alpha\,\rho_m\,(T_\infty - T_1(z))\,z\,dz\,(\varepsilon^2 - 1) = A(\varepsilon^2 - 1)$$

The first term represents the contribution of the crustal root. Here ρ_m and ρ_c are the mantle and crustal densities and h_c the initial crustal thickness. The second term derives from the downward advection of cold material. There, α is the coefficient of thermal expansion, and $T_1(z)$, the initial temperature profile (Figure 5).

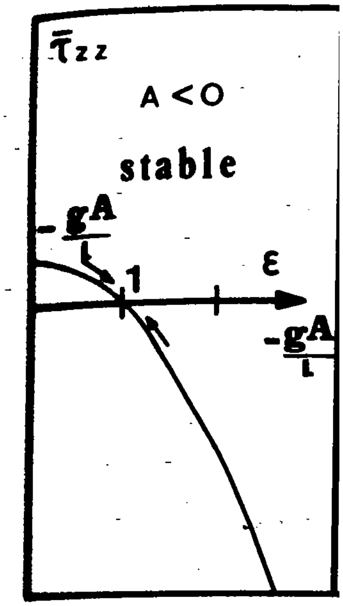

Fig. 6. Lithospheric ave
and adiabatic change in t
implies thickening ; ε <
depending upon the sign o
sign of the density momen
bring the lithosphere bacl
ted by small arrows. Inve

For the simple homogen
process considered here t
cal velocity gradient ∂w/
for the case where τ_{xx} = (

$$\frac{d\varepsilon}{dt} = \gamma A(\varepsilon^2 - 1) = \gamma A(\varepsilon + 1)$$

where $\gamma = g/4\eta\ell$. For an i
predicts the following ti

$$\varepsilon = \frac{1 + e^{2\gamma A t}\left(\frac{\varepsilon_0 - 1}{\varepsilon_0 + 1}\right)}{1 - e^{2\gamma A t}\left(\frac{\varepsilon_0 - 1}{\varepsilon_0 + 1}\right)}$$

When A is negative, i.e.,
thickening (or thinning),
ε = 1, with a time constan
Notice that in this situat

$$\tau_{zz} = \frac{gA}{\ell}(\varepsilon^2 - 1)$$

A far-field horizontal str
to sustain a lithospheric
tity τ_{zz} vs ε is plotted in
case where A is positive,
the thermal root. Any pert
work of this adiabatic mod
is said to be unstable to

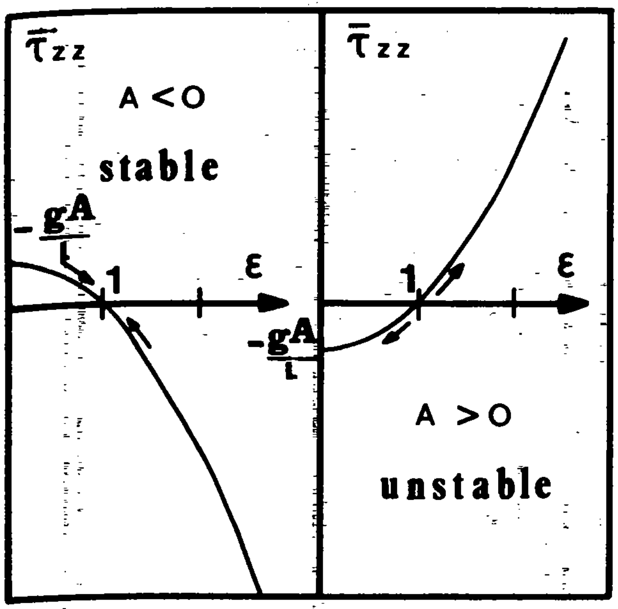

Fig. 6. Lithospheric average vertical stress induced by a homogeneous and adiabatic change in thickness by a factor ε as given by (11) (ε > 1 implies thickening ; ε < 1 implies thinning). Two cases are considered depending upon the sign of A, a parameter defined by (8) and giving the sign of the density moment. For A < 0 the induced stress will tend to bring the lithosphere back to its original thickness (ε = 1), as indicated by small arrows. Inversely the lithosphere is unstable for A > 0.

For the simple homogeneous thickening (ε > 1) - or thinning (ε < 1) - process considered here the thickening rate $\partial\varepsilon/\partial t$ is equal to the vertical velocity gradient $\partial w/\partial z = \partial u/\partial x$. Thus, plugging (8) into (6) one has for the case where $\tau_{xx} = 0$:

$$\frac{d\varepsilon}{dt} = \gamma A(\varepsilon^2 - 1) = \gamma A(\varepsilon + 1)(\varepsilon - 1) \qquad (9)$$

where $\gamma = g/4\eta\ell$. For an initial value ε_o of the deformation this equation predicts the following time evolution of the thickening :

$$\varepsilon = \frac{1 + e^{2\gamma At}\left(\frac{\varepsilon_o - 1}{\varepsilon_o + 1}\right)}{1 - e^{2\gamma At}\left(\frac{\varepsilon_o - 1}{\varepsilon_o + 1}\right)} \qquad (10)$$

When A is negative, i.e., when the dominant effect comes from crustal thickening (or thinning), the lithosphere goes back to its normal state, ε = 1, with a time constant $(-1/2\gamma A)$. The system is said to be stable. Notice that in this situation one has from (3) and (8).

$$\bar{\tau}_{zz} = \frac{gA}{\ell}(\varepsilon^2 - 1) \qquad (11)$$

A far-field horizontal stress $\bar{\tau}_{xx}$ of the same magnitude must be provided to sustain a lithospheric thickening (thinning) of magnitude ε. The quantity $\bar{\tau}_{zz}$ vs ε is plotted in Figure 6. This last figure also depicts the case where A is positive, i.e. where the prevailing influence is due to the thermal root. Any perturbation will tend to grow. Within the framework of this adiabatic model involving a viscous lithosphere the system is said to be unstable to infinitesimal perturbations. It leads to infi-

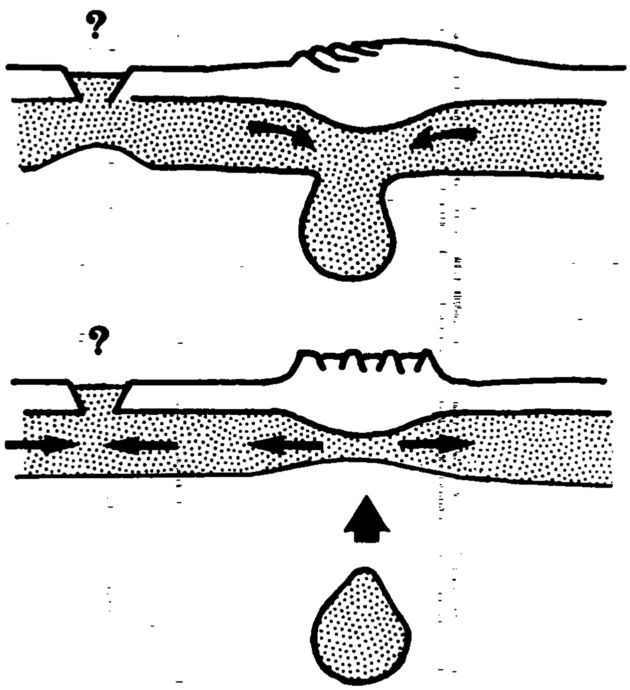

Fig. 7. Schematic picture of the possible time evolution of the lithospheric thickening process. At the top the dense cold lithospheric root generates strong compression in the mountain range. The graben drawn in the periphery may result from the presence of lateral variations of the mechanical properties discussed in section C. At the bottom the instability has gone further : a cold blob has detached so that rapid uplift (thick arrow) is observed in the mountain range, accompanied by extensional tectonics caused by the now predominent mechanical action of the crustal root. Compression may follow in the periphery.

nite thickening, resp. thinning (ridge), after a finite laps of time equal to $1/(2\gamma A) \log [(\varepsilon_0 - 1)/(\varepsilon_0 + 1)]$, resp. $1/(2\gamma A) \log [(1 - \varepsilon_0)/(1 + \varepsilon_0)]$.

What about the sign of A for the continental lithosphere ? Assuming standard values $\rho m - \rho c = 0.5 g/cm^3$, $\rho m = 3.3\ g/cm^3$, $hc = 30$ km, $\alpha = 3\,10^{-5}\ K^{-1}$, and a temperature increasing uniformly to 1400°C with a gradient of 10°C/km one finds that the destabilising influence of the thermal root is about twice as strong as the stabilising effect of the crustal depth variation (equation (8)). Assuming an average lithospheric viscosity $\bar{\eta} = 10^{23}$ poises, one finds a time constant $1/2\ \gamma A$ amounting to 30 Ma. A thicker crust or a thinner thermal lithosphere would yield A values closer to zero or possibly negative. Here one should notice that $A < 0$ implies that, in the region considered, the mechanical state is more extensional than for a ridge (Figure 6). The available data [Richardson et al., 1979] indicate on the contrary that continents are in relative compression when compared with oceanic ridges. The global pattern is discussed elsewhere [L. Fleitout and C. Froidevaux, manuscript in preparation, 1982]. It strengthens the argument that the parameter A is positive almost everywhere in continents.

An adiabatic model, which here predicts that the continental lithosphere is unstable, does not encompass the entire physical picture. On the Earth many continental areas stay stable for hundreds of million years. A variation of the lithospheric thickness certainly induces a temperature anomaly, but the latter can be thermally reequilibrated within a few tens of Ma. Thus after a slow process only the stabilizing crustal density

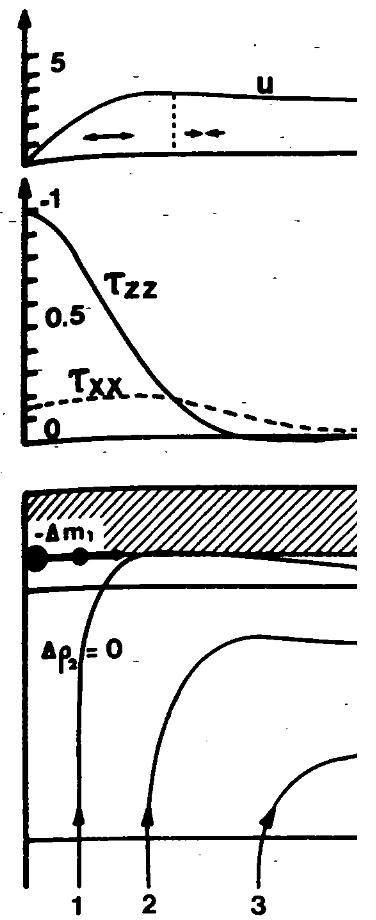

Fig. 8. Plot of the veloci
depth versus distance x fr
The tectonic style depends
small arrows in the top dia
compressional tectonics. Th
in the vertical plane (x, z
model of Figure 1. Here the
lateral extent as suggested
tional to exp. (- $x/0.65\ell_0$)
lower lithosphere ($\Delta\rho$ = 0).
gravity constants equal 1 k
1 kbar. In that case the un
η_0 of layer 4 equals to 10^2

anomaly matters. In cold s
slowly and cannot develop.
nal factor triggers a fini
can be a push or pull tran
of thermal origin : an exa
currents softening the lit
et al., 1981].

Another simplification
of homogeneous thickening
validity of the presented
fails to describe the true

evolution of the litho-
se cold lithospheric root
ange. The graben drawn in
lateral variations of the
At the bottom the instabi-
hed so that rapid uplift
e, accompanied by exten-
mechanical action of the
riphery.

a finite laps of time equal
γA) log [(1 − ε_o)/(1 + ε_o)].
il lithosphere ? Assuming
g/cm^3, hc = 30 km, α = 3 10^{-5}
1400°C with a gradient of
ience of the thermal root is
t of the crustal depth va-
ithospheric viscosity η =
amounting to 30 Ma. A thick-
ld yield A values closer to
tice that A < 0 implies that
e is more extensional than
ichardson et al., 1979] in-
relative compression when
ern is discussed elsewhere
preparation, 1982]. It
is positive almost every-

at the continental lithos-
ire physical picture. On the
hundreds of million years.
tainly induces a temperature
uilibrated within a few tens
bilizing crustal density

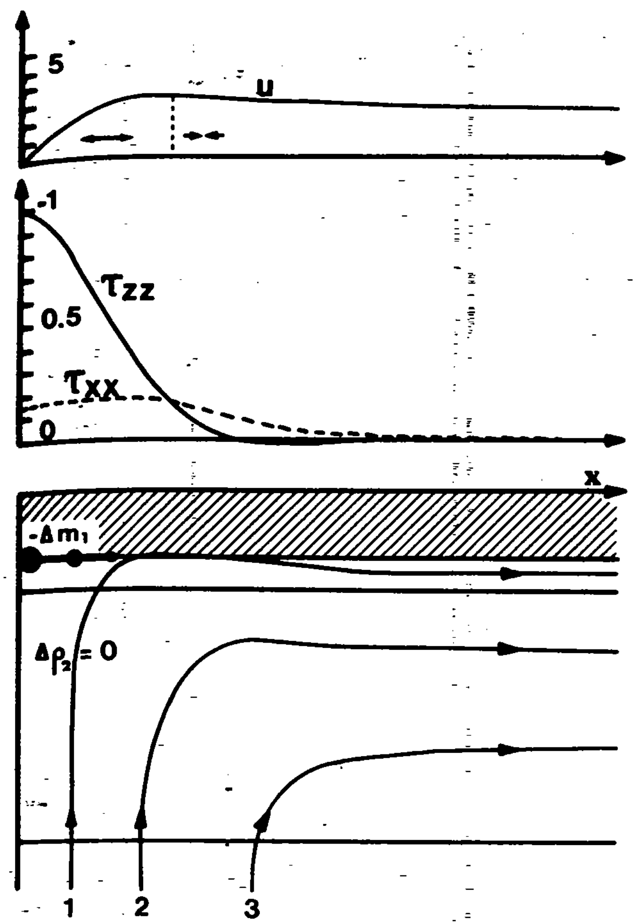

Fig. 8. Plot of the velocity u and of the stress τ_{zz} and τ_{xx} at zero depth versus distance x from the center of an elongated mountain chain. The tectonic style depends upon the sign of ($\tau_{xx} - \tau_{zz}$) or of $\partial u/\partial x$. The small arrows in the top diagram define the regions of extensional or compressional tectonics. The bottom diagram gives the computed flow field in the vertical plane (x, z). It also depicts the chosen lithospheric model of Figure 1. Here the mass heterogeneity at the Moho is of finite lateral extent as suggested by the black beads. Its amplitude is proportional to exp. $(-x/0.65\ell_o)^2$. There is no density heterogeneity in the lower lithosphere ($\Delta\rho$ = 0). If the amplitude of the mass defect times the gravity constants equal 1 kbar, the unit for the stress scale is also 1 kbar. In that case the unit for u amounts to 0.1 mm/yr if the viscosity η_o of layer 4 equals to 10^{23}p and if the reference length ℓ_o equals 100 km.

anomaly matters. In cold strong continental areas perturbations grow slowly and cannot develop. Instabilities will only mature when an external factor triggers a finite amplitude perturbation. The triggering agent can be a push or pull transmitted from a far-field source. It can also be of thermal origin : an example is the action of the upwelling convective currents softening the lithosphere prior to continental break-up [Nataf et al., 1981].

Another simplification introduced in the above model is the assumption of homogeneous thickening or thinning. It does not seriously restrict the validity of the presented arguments about stability, but it certainly fails to describe the true temporal evolution of the process. Unlike the

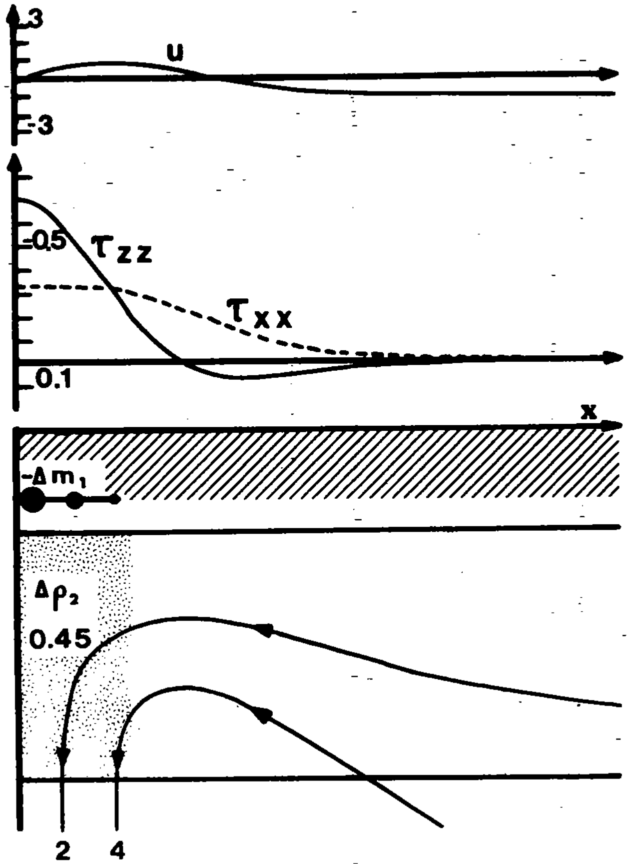

Fig. 9. Similar to Figure 8 but with an additional density heterogeneity located in the lower lithosphere. Its lateral variation is identical to that of Δm and its total mass amounts to $-0.45\ \Delta m$. Notice that the flow line density has been reduced by a factor of 2.

thinning process which can lead to continental break-up, thickening does not go on indefinitely. Both convection experiments [Nataf et al., 1981] and numerical simulations [Houseman et al., 1981] suggest that cold blobs can detach from the upper boundary layer and sink although this process may be hindered somewhat by the strong temperature dependence of the viscosity [Yuen et al., 1981]. A cold lithospheric root could thus break off as shown in Figure 7. Such an event could dramatically hamper the collision process. Tectonic quiescence can in this way follow an orogenic compressive climax.

A full understanding of this whole process requires a thermomechanical treatment. Here we emphasize the idea of a metastable continental lithosphere apt to amplify any large enough heterogeneity. This concept certainly plays a key role in tectonics.

b. Stresses and Velocities for Alpine Type Mountain Chains

The existence of a cold lithospheric root under the Central Alps has raised the question of its role in the mountain building process. Having argued that such a deep thermal structure can maintain the mountain chain in compression, we want to illustrate this point by displaying some simple model solutions. To reflect the evolution of the thermal root during the life of the mountain chain, mass anomalies of various magnitude will be considered. Furthermore the finite width of the structure and possible

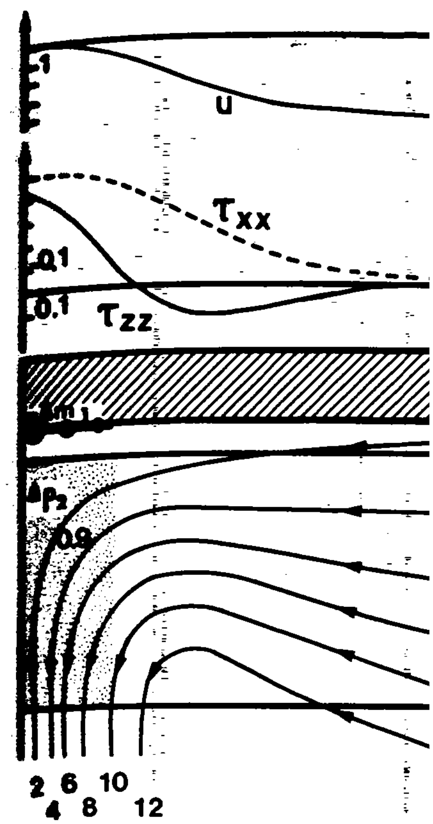

Fig. 10. Similar to Figure 9 but
lower lithosphere amounting to -0

variations in the viscosity profi
ting layered structure is that sh
sity variations are of finite lat
$\Delta m_1 = \partial m_1 \exp(-x^2/d^2)$, and in the
solutions are readily computed by
in section A. The results of such
cally. Each figure present the vi
under consideration. The induced
surface values of the vertical st
the horizontal velocity are plott
topography is proportional to (-τ
$(\partial u/\partial x)$ is indicative of the tect
The asymptotic velocity u is prop
anomalies.

Figures 8, 9 and 10 represent
with three different deep density
(Figure 8) the crustal root provi
topography and the whole structur
in extension. In Figure 9 the col
of the crustal mass deficiency. T
to a 3000 m high mountain with a
60 and 210 km. The moment of the
large scale convergent flow field
mechanical action of the crustal
rating extension in the central z
reinforces the tendency and compr

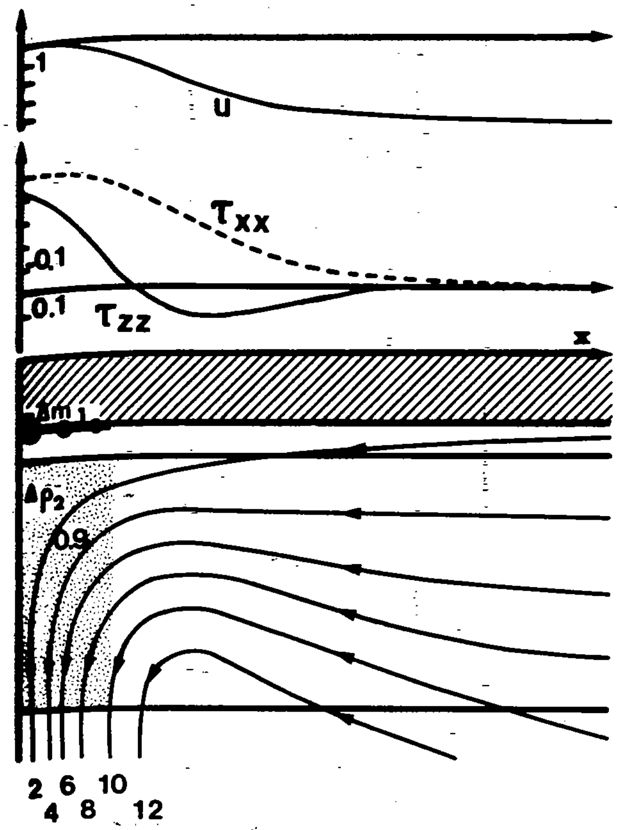

Fig. 10. Similar to Figure 9 but with a density heterogeneity in the lower lithosphere amounting to −0.9 Δm.

variations in the viscosity profile will be taken into account. The starting layered structure is that shown in Figure 1. Now, however, the density variations are of finite lateral extent. At the Moho one has $\Delta m_1 = \partial m_1 \exp(-x^2/d^2)$, and in the fourth layer $\Delta\rho_2 = \partial\rho_2 \exp(-x^2/d^2)$. The solutions are readily computed by superposing harmonic solutions presented in section A. The results of such Fourier integrations are shown graphically. Each figure present the viscosity structure and mass distributions under consideration. The induced flow field overprints this structure and surface values of the vertical stress τ_{zz}, the horizontal stress τ_{xx} and the horizontal velocity are plotted. Here one should remember that the topography is proportional to $(-\tau_{zz})$, and that the sign of $\tau_{xx} - \tau_{zz} = 4\eta (\partial u/\partial x)$ is indicative of the tectonic style (compression or extension). The asymptotic velocity u is proportional to the moment M of the mass anomalies.

Figures 8, 9 and 10 represent the results for a standard lithosphere with three different deep density anomalies. When the latter is absent (Figure 8) the crustal root provides approximate local support for the topography and the whole structure is seen to spread out. The mountain is in extension. In Figure 9 the cold root has a mass excess amounting to 45% of the crustal mass deficiency. This case could, for example, correspond to a 3000 m high mountain with a temperature anomaly of 360° C between 60 and 210 km. The moment of the cold root is dominant. It controls the large scale convergent flow field. At the surface, the more localized mechanical action of the crustal root is, however, still capable of generating extension in the central zone. The denser cold root in Figure 10 reinforces the tendency and compression prevails everywhere at the surface.

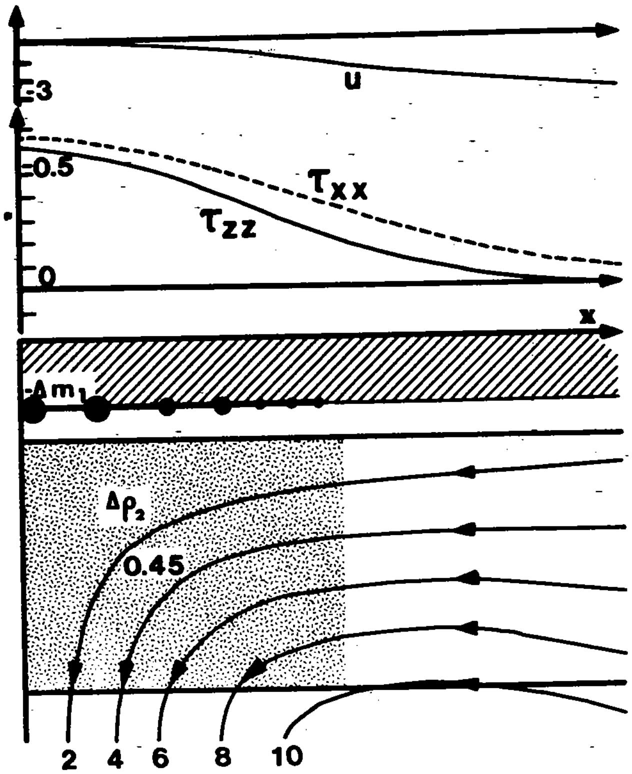

Fig. 11. Similar to Figure 9 but with mass and density heterogeneities extending three times further laterally.

Notice that a density anomaly of finite lateral extent is always fully compensated by the regional topography. The deeper the anomaly the broader the corresponding surface deflection. Hence the presence of a depression next to the mountain in the last two figures. This feature results from viscous flexure.

By comparing Figure 11 to Figure 9 one sees that an increasing width of the density anomaly enhances the dominating influence of the cold root. On the other hand the comparison of Figure 12 to Figure 10 illustrates an opposite effect : the presence of a weak lower crustal layer tends to reestablish extension in the central zone. Such a decoupling layer may well exist in certain geological situations. Looking at the flow fields, one notices that thickening is not homogeneous : the down-going flow is not just fed by lithospheric material but also from upwelling in the asthenosphere. This tendency is enhanced when the viscosity contrast between upper and lower lithosphere is increased. In the limiting case of an elastic upper lithosphere the flow is totally confined to the deeper portion of the structure.

One should specify that all above cases are meant to be idealized illustrations of the effect of a cold root. In realistic situations, lateral mechanical heterogeneities or non-Newtonian rheology can certainly lead to different configurations. The width of the zone in compression could in particular be modified. A particular model is required for each geological case. This is outside the scope of the present paper.

4. THREE DIMENSIONAL DENSITY ANOMALIES AND INTRAPLATE STRESS FIELD

The two dimensional models discussed so far only apply to geological structures with elongated geometries. Two new aspects will now be intro-

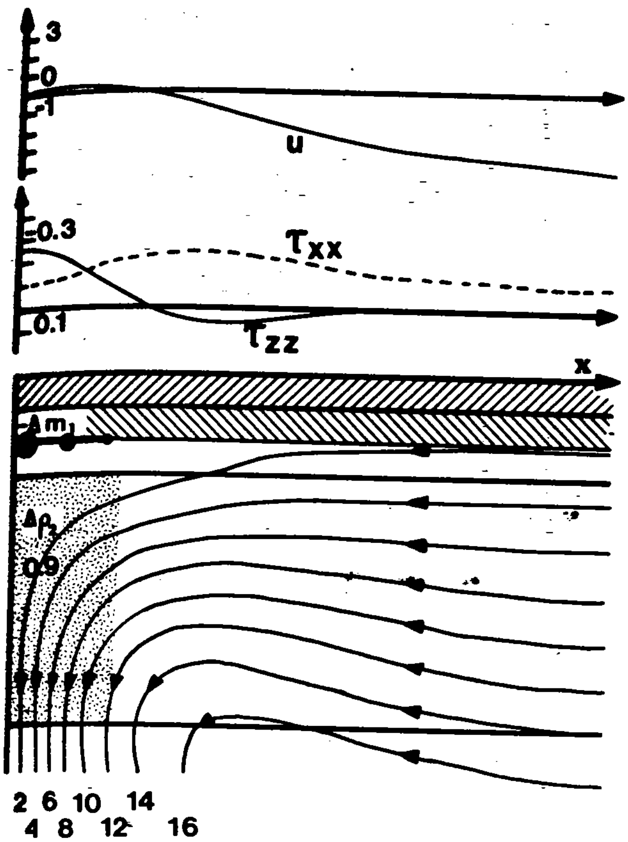

Fig. 12. Similar to Figure 10 but with a lower crust viscosity reduced to $0.1\eta_0$.

duced, which should help to understand regional stress patterns. First, density heterogeneities which vary in two horizontal directions (rather than just one) will be inserted in a stratified lithosphere, where each layer is mechanically homogeneous. Second, allowance will be made for lateral variations of the mechanical properties by considering a case which, in spite of its unsophisticated geometry, will be instructive.

a. Laterally Homogeneous Lithosphere

The mathematical details of the solutions of the Navier-Stokes and continuity equations in a stratified and laterally homogeneous lithosphere are described in appendix 4. Here we shall briefly discuss applications corresponding to the standard viscosity structure of figure 1. The mass heterogeneities, however, are localized in both the x and y direction. At the Moho $\Delta m = \partial m \exp(-x^2/a^2) \exp(-y^2/b^2)$ and in the fourth layer $\Delta\rho = \partial\rho \exp(-x^2/a^2) \exp(-y^2/b^2)$. Velocities and stresses were computed at all depths. In Figure 13 the deviatoric stress pattern and the topography corresponding to four different amplitudes $\partial\rho$ of the cold root have been plotted. The most striking feature is that one cannot predict the relationship between topography and stress regime unless one knows the depth distribution of the density anomalies in the lithosphere. In the center of the figure, the point of highest altitude is seen to be in extension along the shortest axis, in compression along the longest axis or in compression along the shortest axis.

In spite of the additional complexity, these results confirm the gene-

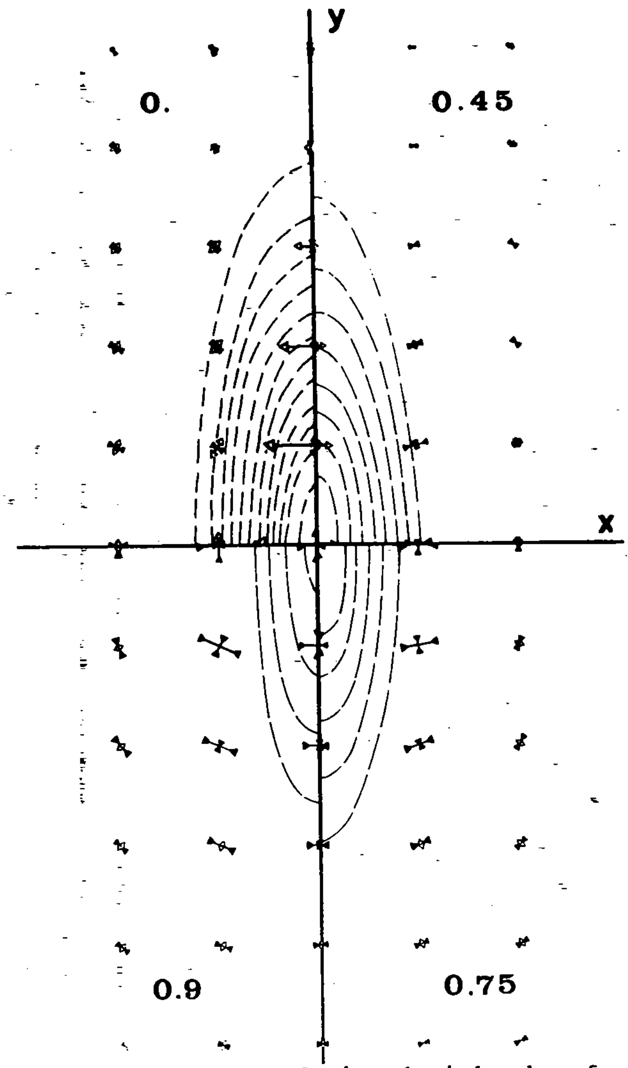

Fig. 13. Four cases showing the induced surface vertical stress (or topography) indicated by the dashed lines as well as the principal horizontal deviatoric stresses indicated by white (extension) or black (compression) arrows. The number in the corner of each diagram is the mass ratio between the mass anomalies in the lower lithosphere and at the Moho. The spacing between leveling lines amounts to 120 bars if Δm_1 corresponds to 1.5 kbar. In this case the scale for the horizontal stresses is such that the extensional τ_{xx} value at the center of the structure, in the upper left quadrant, amounts to 700 b.

ral conclusions obtained with two dimensional models (see figures 8, 9, and 10). Here also, the topography decreases as the intensity of the cold root increases. The material spreads out under the influence of the light crustal root but the presence of a cold root reverses this trend : when the moment M of the density anomalies becomes positive the surrounding lithosphere is attracted towards the mountain. This regional lithospheric thickening is not found to be accompanied by any amount of peripheral lithospheric thinning. This last behavior is a result of our simple assumption of perfect lateral mechanical homogeneity of the structure. Departures from this simplifying assumption will be examined shortly.

b. Comments on Observed Regiona

Let us examine the orientati
region and in Eastern North Ame
mechanisms suggest E-W compress
compression in Western Europe [
et al. 1980]. On the other hand
roughly at right angle to the c
[Zoback and Zoback, 1980]. Alth
rent geodynamical situations we
13 can basically explain both o
The existence of a cold lith
been mentioned already. Its ext
limited [Panza and Mueller, 197
tain chain strikes east-west th
only enhance the prevailing Eur
be attributed to the collision
chain begins to strike southwar
pose a dominant E-W compression.
less convincing.
Let us turn to the Appalachia
pression perpendicular to the str
planation of this stress pattern
root [McNutt, 1980] and, in the
of a partial or total disappeara
suggests that the induced extens
E-W plate compression well docum
course, alternative explanations
cold lithosphere, stresses are l
to erosion could thus cause supe
priate direction [Zoback and Zob

c. Role of Laterally Varying Mec

Let us now come back to the p
13. With a laterally homogeneous
by a three dimensional cold root
foreland but no lithospheric thi
the presence of lateral variatio
a model of extreme geometrical s
cribes three concentric regions
homogeneous density anomaly is l
city we shall assume that its de
This implies that it provides lo
that its moment M is the relevant
formations. Appendix 5 treats thi
tions for mass variations located
When no stresses are applied a
that the same body forces acting
pure strike slip or thickening o
depends in fact upon the relative
ly this is easy to understand. Le
ficiency at depth and a correspon
zone is in extension. For the lim
($\eta_3 >> \eta_2$) zone 2 is compressed b
It thickens. The other limit is t
The spreading out of the central
and thinning of zone 2. The displ
the limiting cases discusses abov
in the appendix. They are plotted
This complex behavior is in co

b. Comments on Observed Regional Stress Fields

Let us examine the orientation of maximum compression in the Alpine region and in Eastern North America. In the Western Alps earthquake focal mechanisms suggest E-W compression, in contrast to the prevailing N-S compression in Western Europe [Fréchet, 1978 ; Philip, 1980 ; Froidevaux et al. 1980]. On the other hand the compression in the Appalachians is roughly at right angle to the compression in the surrounding regions [Zoback and Zoback, 1980]. Although these two examples represent diffe-rent geodynamical situations we think that the models presented in Figure 13 can basically explain both observed stress patterns.

The existence of a cold lithospheric root under the Central Alps has been mentioned already. Its extension under the Western Alps seems to be limited [Panza and Mueller, 1979 ; Poupinet, 1976]. As long as the mountain chain strikes east-west the predicted north-south compression can only enhance the prevailing European long range stress field, which should be attributed to the collision with Africa [Froidevaux et al., 1978]. As the chain begins to strike southward the effect of the cold root is to superpose a dominant E-W compression. In the southern branch the field data is less convincing.

Let us turn to the Appalachians. Here the salient feature is that compression perpendicular to the strike of the structure seems reduced. The explanation of this stress pattern makes use of the existence of a crustal root [McNutt, 1980] and, in the consideration of the age of this orogeny, of a partial or total disappearance of the cold lithospheric root. It suggests that the induced extensional stress somewhat cancels out the E-W plate compression well documented on the eastern border. Here, of course, alternative explanations can be put forward : in a relatively cold lithosphere, stresses are less liable to relax, and uplift related to erosion could thus cause superficial flexural extension in the approprfate direction [Zoback and Zoback, 1980].

c. Role of Laterally Varying Mechanical Properties

Let us now come back to the point raised in the discussion of Figure 13. With a laterally homogeneous lithosphere, regional thickening induced by a three dimensional cold root generates strike-slip deformation in the foreland but no lithospheric thinning. This assertion does not hold in the presence of lateral variations of the viscosity. To demonstrate this, a model of extreme geometrical simplicity is sufficient. Figure 14 describes three concentric regions of different viscosities. A laterally homogeneous density anomaly is located in the central zone. For simplicity we shall assume that its depth is smaller than its lateral extent. This implies that it provides local compensation for the topography and that its moment M is the relevant quantity for describing mechanical deformations. Appendix 5 treats this problem and derives analytical solutions for mass variations located at the base of the lithosphere ($M=\partial mgh$).

When no stresses are applied at infinity the most salient feature is that the same body forces acting in the central zone can generate either pure strike slip or thickening or thinning in zone 2. This tectonic style depends in fact upon the relative viscosities in zones 2 and 3. Physically this is easy to understand. Let us assume a central negative mass deficiency at depth and a corresponding high topography (plateau). This zone is in extension. For the limiting case of a rigid outer region ($\eta_3 \gg \eta_2$) zone 2 is compressed by the spreading of the central plateau. It thickens. The other limit is that of an inviscid outer reion ($\eta_3 \ll \eta_2$). The spreading out of the central plateau causes the geometric expansion and thinning of zone 2. The displacement velocity and deformations for the limiting cases discusses above can be derived from expressions found in the appendix. They are plotted in Figure 15.

This complex behavior is in contrast with that of an equivalent two

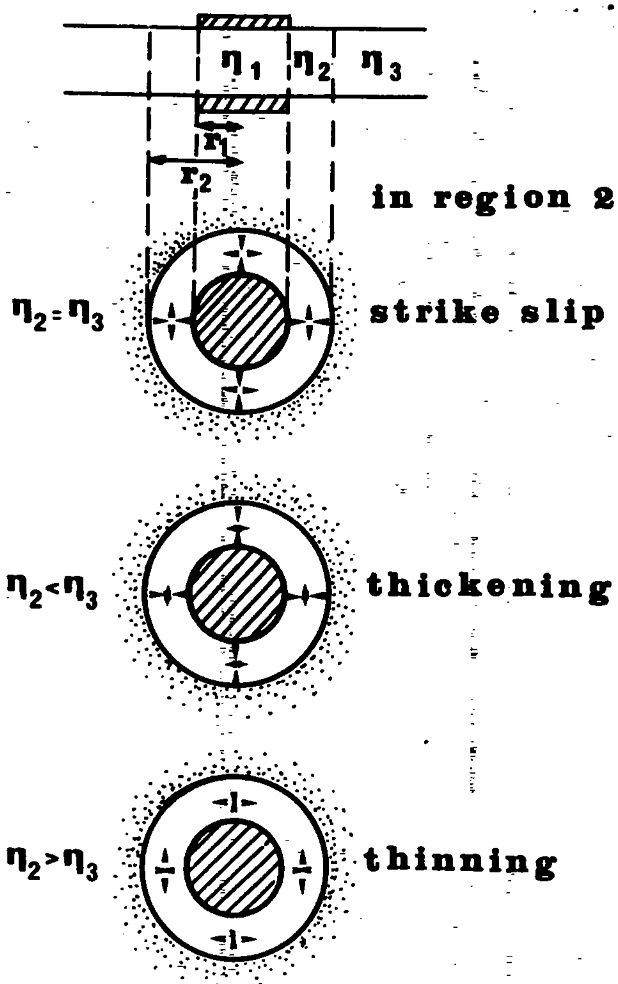

Fig. 14. Three concentric regions with different viscosities η_1, η_2 and η_3 with a compensated load applied to the central region. The top diagram is a vertical cross section and the three maps underneath illustrate three possible tectonic styles in the intermediate region (small arrows).

dimensional model (infinitely elongated plateau), where extension of the central zone displaces but does not deform the neighbouring regions. Indeed in two-dimensional models the deformation is determined only by local density variations and mechanical properties.

Another useful comparison between three -and two- dimensional structures can be made by raising the following question : what stresses must be applied at large distance to keep an elevated plateau from spreading ? In two-dimensional models this requires $\bar{\tau}_{xx} = \bar{\tau}_{zz}$, which according to (3) implies a far-field horizontal stress $\bar{\tau}_{xx}$ totally independent of the mechanical properties of the lithosphere. In three dimensions the simple concentric model of Figure 14 shows that the far-field stress capable of sustaining the central topographic structure strongly depends upon the relative viscosities of zones 3 and 2 (see equation (E20).Clearly in the extreme case of a rigid outer region the geometrical configuration shows that no finite far-field stress is capable of inducing a deformation of the intermediate zone 2. Only such deformation could transmit stress to the central zone, so that a deformable outer zone is required. However, the more viscous this outer zone, the larger the required far-field stress.

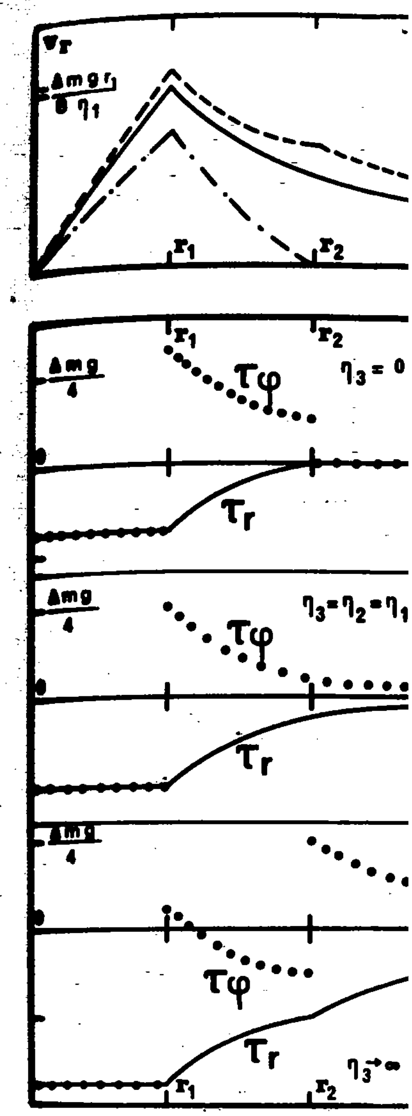

Fig. 15. Plots of the radial v
ric regions depicted in Figure
same viscosities ($\eta_1 = \eta_2$). Th
dered for the external zone. Th
radial velocity v_r correspond t
given underneath. τϕ (dotted li

This last conclusion indicat
sation of stable large geologic
a reliable indicator or gauge c
a more general sense, the compu
makes one face the formidable r
of compensation of the topograp
erogeneities) but also the late
of the whole lithosphere. Possi
ances can give rise to a large
nics. An illustration can be fo
the lithosphere towards the mou

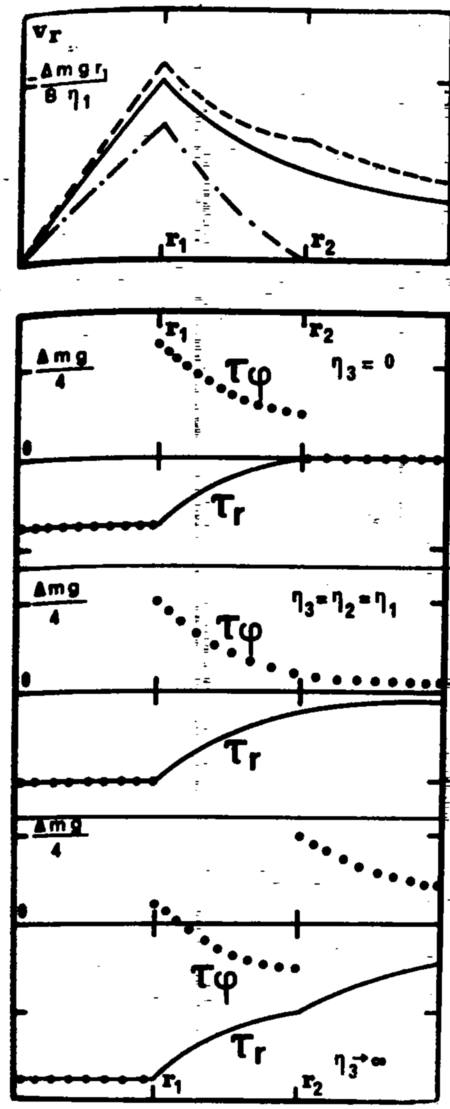

Fig. 15. Plots of the radial velocity and horizontal stresses in concentric regions depicted in Figure 14. Here the two central zones have the same viscosities ($\eta_1 = \eta_2$). Three different values of η_3 have been considered for the external zone. The top, middle and lower curve for the radial velocity v_r correspond to the top, middle and lower stress graphs given underneath. $\tau\phi$ (dotted line) and τ_r (full line) are plotted versus r.

This last conclusion indicates that the elevation and depth of compensation of stable large geological structures do not constitute in general a reliable indicator or gauge of the stress intensity in the foreland. In a more general sense, the computation of the stress field in a given area makes one face the formidable requirement of knowing not only the depth of compensation of the topography (i.e. of the moment M of the mass heterogeneities) but also the lateral variations of the mechanical properties of the whole lithosphere. Possible interactions between different provinces can give rise to a large variety of phenomena in continental tectonics. An illustration can be found in Figure 13 where the inward flow of the lithosphere towards the mountain structure could very well be accompanied by thinning if zones of mechanical weakness exist in the foreland. Such low strength regions are predicted when non-Newtonian effects are taken into account. Another source of weakening derives from induced warm upwelling currents such as those pictured on Figure 10. Extensional structures around the Alpine chain in Europe could have been formed in this manner.

The concept of stresses due to lithospheric density heterogeneities emphasized in this paper does not contradict the widespread belief in a "far field transmitted stress field" which is the consequence of more or less distant sources. For example, although compressional tectonics in Asia must be helped by the "cold root effect" which must exist in any collision process, some compression is certainly also caused by the Indian plate subducting under Indonesia.

5. DISCUSSION AND CONCLUSION

This paper puts forward a physical framework for the analysis of intraplate deformations caused by existing density heterogeneities within the lithosphere. For long wavelength density variations, the lithospheric thickening or thinning rate was shown to be proportional to the local moment of the density anomalies. For elongated structures, this golden rule applies whatever the type and spatial variations of the mechanical properties. It explains observed tectonic stresses related to large scale structural units. Deeply compensated ridges and elevated rifted regions are thus in extension, but high moutains compensated not only by a light crustal root but also by a deeper lithospheric cold root are in compression. For short wavelength density variations, the lithospheric deformation varies with depth. For instance, in a narrow moutain range extension can occur in the crust although just below a convergent flow is induced in the lower lithosphere by the dense cold root. Density heterogeneities of short lateral extent are regionally, but not locally compensated by topography. The larger the wavelength, the stronger the local component of the compensation.

The calculation of intraplate deformations and stress patterns must take into account the existence of lateral variations of the mechanical properties. This reveals important geometrical constraints leading to a coupling in the deformation of adjacent provinces. For example, regional lithospheric thickening can be accompanied by peripheral extension. Three dimensional tectonic models must specify not only the topography and its compensation depth, but also the mechanical heterogeneities of the lithosphere. In the present stage of knowledge this is not an easy task. Conversely, observed regional stress fields can provide a hint about deep seated density variations and about mechanical heterogeneities. This approach was illustrated by relating rapid changes of the stress orientations in the Alps or the Appalachians to the predominance either of a dense cold root or a light crustal root. More generally, tectonic stress patterns combined with other geophysical data (seismic structure, gravimetry anomalies, heat flow) should become a useful element of the dataset, from which to infer the deep lithospheric structure.

a. Rheology

The mathematical treatment of the lithospheric deformation is very simple for the case of a Newtonian viscosity. This simplicity justifies the starting assumptions of our models. It gives optimum physical insight as the use of the superposition principle allows one to investigate separately the solutions for each wavelength and to obtain simple analytical formulations. This approach is adequate for the understanding of general phenomena. Regional studies deserve the introduction of further improvements and complications : non Newtonian behavior, presence of shear zones, etc.

Why do we emphasize model
layer ? Truly the Earth's li
This paper showed that the c
ical whether the upper layer
in an elastic upper lithosph
ing deformations are of negl
or creation of a 10 km defle
of the order of 30 %. This i
strain amouting to 10^{-3}. If
place rapidly, say in 10 Ma,
cosity not exeeding 10^{24}p. T
ence of various deformation
shear zones. Its magnitude s
viscosity contrats chosen fo

b. Depth Range for Density A

This paper has analyzed t
various intraplate deformati
density anomalies capable of
this limit goes beyond what
lithosphere. As long as the
is slowed down by viscous str
deflection of the Earth's su
down the same mass heterogen
by the local flow it may ind
a lower boundary. This latte
our models, and, as an examp
the lithospheric thickening
valid. In the Earth it seems
the lithosphere to some 200
subduction. This process has
sion. However, the stress st
shows that its deepest portic

c. Tectonic Phases : Some Spe

The lithospheric stresses
paper derive from the instant
phere to prescribed density v
been considered. This would r
the thermal density anomalies
does not preclude some qualit
of a mountain chain. We showe
come unstable if it suffers a
itial thickening of moderate
itself thanks to the sinking
root will then grow and ampli
stresses will typically reach
high tectonic activity accomp
folding.

The models predict two dis
cold root can generate a down
mountain range. Hence the exi
tains. This flexural trough i
existing molasse filled depre
be induced in zones of weakne
triggered and will mature aft
eral rifts is probably essent
geneities of the lithosphere.
very elongated system of exte

Why do we emphasize models with a viscous rather than elastic upper layer ? Truly the Earth's lithosphere can exhibit an elastic behavior. This paper showed that the computed mean horizontal stresses are identical whether the upper layer is elastic or viscous (appendix 2). Stresses in an elastic upper lithosphere are of no interest here as the corresponding deformations are of negligible magnitude. For comparison the removal or creation of a 10 km deflection at the Moho gives rise to crustal strains of the order of 30 %. This is much larger than the resulting elastic strain amouting to 10^{-3}. If this variation in crustal thickness takes place rapidly, say in 10 Ma, the deformed lithosphere has an average viscosity not exeeding 10^{24}p. This low viscosity integrates in fact the presence of various deformation processes including rapid creep in localized shear zones. Its magnitude somewhat justifies the relatively moderate viscosity contrats chosen for our "standard model" (Figure 1).

b. Depth Range for Density Anomalies

This paper has analyzed the role of existing density anomalies in various intraplate deformation processes. Is there a depth limit for the density anomalies capable of entering our models ? The answer is yes, but this limit goes beyond what is usually considered as the bottom of the lithosphere. As long as the motion of a mass heterogeneity in the mantle is slowed down by viscous stresses supported from above, it induces a deflection of the Earth's surface, which compensates its weight. Further down the same mass heterogeneity becomes partially supported from below by the local flow it may induce and by pressure forces as it approaches a lower boundary. This latter case is definitely outside of the scope of our models, and, as an example, the relationship between the moment M and the lithospheric thickening rate does not apply because (2) is non longer valid. In the Earth it seems reasonable to limit the zone of influence of the lithosphere to some 200 or 300 km. An illustration is found in oceanic subduction. This process has some common features with continental collision. However, the stress state of the slab [Isacks and Molnar, 1971] shows that its deepest portions may be supported from below.

c. Tectonic Phases : Some Speculations

The lithospheric stresses and deformations computed throughout this paper derive from the instantaneous mechanical response of a model lithosphere to prescribed density variations. The temporal evolution has not been considered. This would require a thermo-mechanical treatment, where the thermal density anomalies are also time dependent. This limitation does not preclude some qualitative statements concerning the evolution of a mountain chain. We showed that the continental lithosphere can become unstable if it suffers a finite rapid perturbation. Thus after initial thickening of moderate amplitude the collision process can sustain itself thanks to the sinking tendency of the cold lithospheric root. This root will then grow and amplify the regional compression. The induced stresses will typically reach 1 kbar. The mountain is in its phase of high tectonic activity accompanied by emplacement of nappes and intense folding.

The models predict two distinct structures in the foreland. First, the cold root can generate a downward surface deflection broader than the mountain range. Hence the existence of a subsided zone close to the mountains. This flexural trough is in compression and could correspond to existing molasse filled depressions. Secondly extensional tectonics can be induced in zones of weakness. There, thinning instabilities can be triggered and will mature after some delay. The geometry of these peripheral rifts is probably essentially controlled by the mechanical heterogeneities of the lithosphere. The grabens around the Alps belong to a very elongated system of extension between the North Sea and the Mediterranian. However the Alpine collision zone is certainly linked to their formation .

At the climax of the compressional phase the altitude remains moderate because of the presence of the cold-root. If the latter stops growing, its slow warming-up will generate uplift during some tens of Ma. A more dramatic event takes place if the cold root grows large enough to break off and sink. The overlying region will experience rapid uplift without compression. The elevated structure will even be in extension now that the dense lithospheric root has disapeared. If Tibet has raised in a relatively short time, it could be a good candidate for the above mechanism. Such a scenario may have some similarity with the proposed delamination event for the Colorado plateau [Bird and Baumgardener, 1981]

In conclusion, this paper should help to dismiss the picture of the continental lithosphere reacting passively to external push or pull. The proposed physical concept suggests a dynamic structure where local sources and neighbouring activity generate a great wealth of internal tectonic phenomena.

APPENDIX 1 : MATHEMATICAL RESOLUTION FOR A HARMONIC PERTURBATION

Let us consider a two-dimensional layered structure similar to the model lithosphere pictured in Figure 1. Each layer has a uniform Newtonian viscosity. In some cases, however, an elastic top layer is added. Mass heterogeneities are either located at the interface between two layers or distributed homogeneously with the depth z in a single layer. The amplitude of these mass fluctuations is a harmonic function of the horizontal direction : $\Delta\rho = \delta\rho\cos(kx)$ for distributed density heterogeneities and $\Delta m = \delta m\cos(kx)$ for mass heterogeneities concentrated at an interface.

The induced velocity and stress fields are computed by solving the Navier-Stokes and continuity equations. For a given layer these equations read :

$$\eta\left(\frac{\partial^2 u}{\partial x^2} + \frac{\partial^2 u}{\partial z^2}\right) = \frac{\partial p}{\partial x} \qquad \text{(A1)}$$

$$\eta\left(\frac{\partial^2 w}{\partial x^2} + \frac{\partial^2 w}{\partial z^2}\right) = \frac{\partial p}{\partial z} - \Delta\rho g \qquad \text{(A2)}$$

$$\frac{\partial u}{\partial x} + \frac{\partial w}{\partial z} = 0 \qquad \text{(A3)}$$

Where u and w are the horizontal velocity components, g is the gravity acceleration, and p is the departure from the hydrostatic pressure. The standard procedure is that used for solving the post-glacial rebound problem in a layered Earth [Takeuchi and Hasegawa, 1965 ; Lliboutry, 1973; Cathles, 1975] or the more general viscous flow problem for the Earth's mantle [Hager and O'Connell, 1981]. The unknown functionals can be written in a harmonic form :

$$u = h(z)\sin(kx) \qquad \text{(A4)}$$
$$w = j(z)\cos(kx) \qquad \text{(A5)}$$
$$p = p(z)\cos(kx) \qquad \text{(A6)}$$

Inserting these functions into (A1), (A2), and (A3) one finds the following relations :

$$\frac{d^2h}{dz^2} - k^2 h = -\frac{kp}{\eta} \qquad \text{(A7)}$$

$$\frac{d^2j}{dz^2} - k^2 j = \left[\frac{dp}{dz} - \partial\rho g\right]\frac{1}{\eta}$$

$$\frac{dj}{dz} + kh = 0$$

These can be combined to f
volving only j(z) :

$$\frac{d^4j}{dz^4} - 2k^2\frac{d^2j}{dz^2} + k^4 j - k^2\frac{\partial\rho g}{\eta}$$

The general solution can b

$$j = (A + Bkz)\,e^{kz} + (C + Dkz)$$

where A, B, C, and D are const
tions h(z) and p(z) can easily
(A7) and (A9) :

$$h = -(A + B + Bkz)\,e^{kz} + (C - $$

$$p = 2\eta k(Be^{kz} + De^{-kz})$$

Furthermore the nonhydrostat
$\tau_{zz} = 2\eta(\partial w/\partial z) - p$ and $\tau_{xz} = \eta$
ted :

$$\tau_{xx} = 2\eta k\left(-(A + 2B + Bkz)\,e^{kz} + \right.$$

$$\tau_{zz} = 2\eta k\left((A + Bkz)\,e^{kz} - (C + \right.$$

$$\tau_{xz} = \left(-2\eta k((A + B + Bkz)\,e^{kz} + \right.$$

Positive stress values corres
is thus solved. The exact values
D in each layer depend on the bo
lations at interfaces between la
extends to infinity. In this lay
and stresses remain finite at la
for the constants in the top lay
city (w = 0) and either free sli
surface.

Finally, at each interface be
the stresses τ_{xz} and τ_{zz} must be
when a mass heterogeneity ∂m is
jump ∂mg in the value of τ_{zz}. Alt
the 4n integration constants corr

The results can be presented i
as references a length ℓ_o, a visc
sional quantities are denoted by

$k' = k\ell_o$
$\eta' = \eta/\eta_o$
$\partial\rho' = \partial\rho/\partial\rho_o$

certainly linked to their
ıe altitude remains moderate
.he latter stops growing, its
ıme tens of Ma. A more drama-
arge enough to break off
rapid uplift without com-
in extension now that the
et has raised in a relative-
r the above mechanism. Such
roposed delamination event
:r, 1981]
smiss the picture of the
external push or pull. The
tructure where local sources
lth of internal tectonic

MONIC PERTURBATION

tructure similar to the
ayer has a uniform Newto-
stic top layer is added.
nterface between two layers
in a single layer. The am-
ic function of the horizon-
ed density heterogeneities
ncentrated at an interface.
computed by solving the
given layer these equations

(A1)

(A2)

(A3)

nents, g is the gravity
ydrostatic pressure. The
post-glacial rebound
wa, 1965 ; Lliboutry, 1973;
problem for the Earth's
functionals can be written

(A4)
(A5)
(A6)

ıd (A3) one finds the fol-

(A7)

$$\frac{d^2j}{dz^2} - k^2 j = \left[\frac{dp}{dz} - \partial\rho g\right]\frac{1}{\eta} \qquad \text{(A8)}$$

$$\frac{dj}{dz} + kh = 0 \qquad \text{(A9)}$$

These can be combined to form a fourth order differential equation involving only j(z) :

$$\frac{d^4j}{dz^4} - 2k^2\frac{d^2j}{dz^2} + k^4 j - k^2\frac{\partial\rho g}{\eta} = 0 \qquad \text{(A10)}$$

The general solution can be written in the following form :

$$j = (A + Bkz)\,e^{kz} + (C + Dkz)\,e^{-kz} + \frac{\partial\rho g}{\eta k^2} \qquad \text{(A11)}$$

where A, B, C, and D are constants for a given layer. The two other functions h(z) and p(z) can easily be derived by substitution of (A11) in (A7) and (A9) :

$$h = -(A + B + Bkz)\,e^{kz} + (C - D + Dkz)\,e^{-kz} \qquad \text{(A12)}$$

$$p = 2\eta k(Be^{kz} + De^{-kz}) \qquad \text{(A13)}$$

Furthermore the nonhydrostatic stresses $\tau_{xx} = 2\eta(\partial u/\partial x) - p$, $\tau_{zz} = 2\eta(\partial w/\partial z) - p$ and $\tau_{xz} = \eta(\partial u/\partial z + \partial w/\partial x)$ are also readily calculated :

$$\tau_{xx} = 2\eta k\left(-(A + 2B + Bkz)\,e^{kz} + (C + Dkz - 2D)\,e^{-kz}\right)\cos(kx) \qquad \text{(A14)}$$

$$\tau_{zz} = 2\eta k\left((A + Bkz)\,e^{kz} - (C + Dkz)\,e^{-kz}\right)\cos(kx) \qquad \text{(A15)}$$

$$\tau_{xz} = \left(-2\eta k\left((A + B + Bkz)\,e^{kz} + (C - D + Dkz)\,e^{-kz}\right) - \frac{\partial\rho g}{k}\right)\sin(kx) \qquad \text{(A16)}$$

Positive stress values correspond to extension. Formally, the problem is thus solved. The exact values of the integration constants A, B, C and D in each layer depend on the boundary conditions and the continuity relations at interfaces between layers. In all our models the lowest layer extends to infinity. In this layer one has A = B = 0 so that velocities and stresses remain finite at large depth. Two more relations are derived for the constants in the top layer by assuming a vanishing vertical velocity (w = 0) and either free slip ($\tau_{xz} = 0$) or no slip (u = 0) at the surface.

Finally, at each interface between layers the velocities u and w and the stresses τ_{xz} and τ_{zz} must be continuous. There is now one exception when a mass heterogeneity ∂m is found at the interface. This requires a jump $\partial m g$ in the value of τ_{zz}. Altogether one has 4 n relationships between the 4 n integration constants corresponding to a n layer model.

The results can be presented in a nondimensional form by introducing as references a length ℓ_o, a viscosity η_o, and a density $\partial\rho_o$. Nondimensional quantities are denoted by primes as follows :

$$k' = k\ell_o$$
$$\eta' = \eta/\eta_o$$
$$\partial\rho' = \partial\rho/\partial\rho_o$$

$$u' = \frac{u\,\eta_o}{\partial\rho_o\, g\, \ell_o^2} \qquad \text{(A17)}$$

$$v' = \frac{v\,\eta_o}{\partial\rho_o\, g\, \ell_o^2}$$

$$\tau' = \tau/\partial\rho_o\, g\, \ell_o$$

From this one may infer that the dimensional velocities are proportional to the square of the characteristic dimension of the system ℓ_o. On the other hand, the stress magnitude is independent of the value of the reference viscosity η_o, although it does depend upon the viscosity ratios between layers.

APPENDIX 2 : ANALYTICAL SOLUTIONS FOR SOME ELEMENTARY STRUCTURES

Case I : Simple Half-Space Model

Let us consider a sinusoidal mass heterogeneity ∂m at a depth d in a viscous medium (Figure A1). The top part of thickness d will be called layer 1 and the half-space underneath it, layer 2. The viscosity contrast η_2/η_1 equals μ. The integration constants in (A11) shall be written with index 1, resp. 2.

Following (A11) and (A16) one can express that both the vertical velocity and the shear stress vanish at z = 0. This yields :

$$A_1 + C_1 = 0 \qquad \text{(B1)}$$

$$A_1 + B_1 + C_1 - D_1 = 0 \qquad \text{(B2)}$$

The conditions at infinity imply :

$$A_2 = B_2 = 0 \qquad \text{(B3)}$$

and finally at the interface (z = d) continuity in velocities expressed by (A11) and (A12) and in stresses expressed by (A15) and (A16) leads to the additional relationships :

$$(A_1 + B_1\, kd)\, e^{kd} + (C_1 + D_1\, kd)\, e^{-kd} = (C_2 + D_2\, kd)\, e^{-kd} \qquad \text{(B4)}$$

$$-(A_1 + B_1 + B_1 kd)\, e^{kd} + (C_1 - D_1 + D_1 kd)\, e^{-kd} = (C_2 - D_2 + D_2 kd) e^{-kd} \qquad \text{(B5)}$$

$$(A_1 + B_1 + B_1 kd)\, e^{kd} + (C_1 - D_1 + D_1 kd)\, e^{-kd} = \mu(C_2 - D_2 + D_2 kd) e^{-kd} \qquad \text{(B6)}$$

$$(A_1 + B_1 kd)\, e^{kd} - (C_1 + D_1 kd)\, e^{-kd} = -\mu(C_2 + D_2 kd)\, e^{-kd} + \frac{\partial mg}{2\eta k} \qquad \text{(B7)}$$

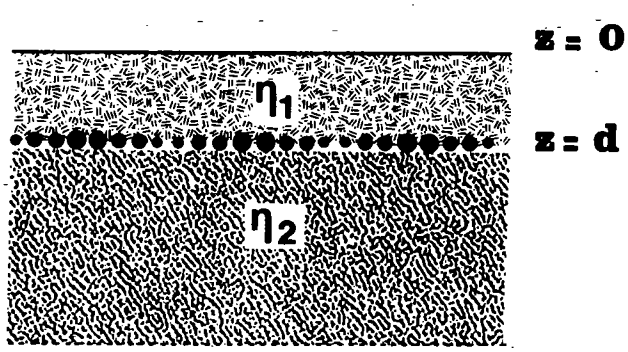

Fig. A1. Simple two layered structure with top layer of viscosity η_1 and an infinite lower layer of viscosity η_2. A harmonic distribution of mass is located at the interface.

The above system of equa
integration. Here we shall
ratio : μ = 1 and μ = 0.
For μ = 1 one has an infi
solutions read as follow :

$$A_1 = \frac{\partial mg}{4\eta k}(1 + kd)\, e^{-kd}$$

$$B_1 = -\frac{\partial mg}{4\eta k}\, e^{-kd}$$

$$C_1 = -\frac{\partial mg}{4\eta k}(1 + kd)\, e^{-kd}$$

$$D_1 = -\frac{\partial mg}{4\eta k}\, e^{-kd}$$

$$C_2 = \frac{\partial mg}{4\eta k}(e^{kd} - e^{-kd}) + kd(e \ldots$$

$$D_2 = -\frac{\partial mg}{4\eta k}(e^{kd} - e^{-kd})$$

All physical quantities
values of the horizontal vel
(z = 0). Substituting (B8) i

$$u = -\frac{\partial mgd}{2\eta}\sin(kx)$$

$$\tau_{zz} = \partial mg(1 + kd)\, e^{-kd}\cos(kx$$

$$\tau_{xx} = \partial mg(1 - kd)\, e^{-kd}\cos(kx$$

Figure A2 in the left por
The first quantity is proporti
wavelengths it has its maximu
topography is exactly compens
falling off of the curve at s
local compensation does not h
tity is the difference (τ_{xx} -
formation $\partial u/\partial x$ at the surfac
surprising. We shall see that
having a reduced viscosity in

Case II : Simple Plate Model

This case differs from the
pect : layer 2 has a vanishing
hold and must be combined with
member equal to zero as η_2 van

$$A_1 = \frac{\partial mg}{4\eta k}\, \frac{kd\cosh(kd) + \sinh(k}{kd + \sinh(kd)\cosh(k}$$

$$B_1 = \frac{\partial mg}{4\eta k}\, \frac{\sinh(kd)}{\sinh(kd)\cosh(kd) + }$$

$$C_1 = \frac{\partial mg}{4\eta k}\, \frac{kd\cosh(kd) + \sinh(k}{kd + \sinh(kd)\cosh(}$$

$$D_1 = -\frac{mg}{4\,k}\, \frac{\sinh(kd)}{\sinh(kd)\cosh(kd)}$$

and the surface values of stre

The above system of equations defines the values of all constants of integration. Here we shall treat two specific values of the viscosity ratio : $\mu = 1$ and $\mu = 0$.

For $\mu = 1$ one has an infinite half-space of constant viscosity. The solutions read as follow :

$$A_1 = \frac{\partial mg}{4\eta k} (1 + kd)\, e^{-kd}$$

$$B_1 = - \frac{\partial mg}{4\eta k} e^{-kd}$$

$$C_1 = - \frac{\partial mg}{4\eta k} (1 + kd)\, e^{-kd}$$

$$D_1 = - \frac{\partial mg}{4\eta k} e^{-kd}$$

$$C_2 = \frac{\partial mg}{4\eta k} (e^{kd} - e^{-kd}) + kd(e^{kd} - 3e^{-kd}) \qquad (B8)$$

$$D_2 = - \frac{\partial mg}{4\eta k} (e^{kd} - e^{-kd})$$

All physical quantities are now defined. We shall discuss and plot the values of the horizontal velocity and normal stresses at the surface ($z = 0$). Substituting (B8) in (A12), (A14), and (A15) one finds :

$$u = - \frac{\partial mgd}{2\eta} \sin(kx) \qquad (B9)$$

$$\tau_{zz} = \partial mg(1 + kd)\, e^{-kd} \cos(kx) \qquad (B10)$$

$$\tau_{xx} = \partial mg(1 - kd)\, e^{-kd} \cos(kx) \qquad (B11)$$

Figure A2 in the left portion depicts the amplitude of τ_{zz} and τ_{xx}. The first quantity is proportional to the induced topography. At large wavelengths it has its maximum value which implies that the weight of the topography is exactly compensated by the mass defect ∂m at depth. The falling off of the curve at shorter wavelength (large k) shows that local compensation does not hold in that case. The other meaningful quantity is the difference $(\tau_{xx} - \tau_{zz}) = 4\eta(\partial u/\partial x)$. It characterizes the deformation $\partial u/\partial x$ at the surface. Its vanishing at large wavelength may be surprising. We shall see that this case is somewhat pathological for not having a reduced viscosity in the lower layer.

Case II : Simple Plate Model

This case differs from the previous one (Figure A1) only in one aspect : layer 2 has a vanishing viscosity. Equations (B1) and (B2) still hold and must be combined with equations (B6) and (B7) which have a right member equal to zero as η_2 vanishes. Thus one finds :

$$A_1 = \frac{\partial mg}{4\eta k} \frac{kd \cosh(kd) + \sinh(kd)}{kd + \sinh(kd)\cosh(kd)}$$

$$B_1 = \frac{\partial mg}{4\eta k} \frac{\sinh(kd)}{\sinh(kd)\cosh(kd) + dk}$$

$$C_1 = \frac{\partial mg}{4\eta k} \frac{kd \cosh(kd) + \sinh(kd)}{kd + \sinh(kd)\cosh(kd)} \qquad (B12)$$

$$D_1 = - \frac{mg}{4\,k} \frac{\sinh(kd)}{\sinh(kd)\cosh(kd) + kd}$$

and the surface values of stress and horizontal velocity are expressed by:

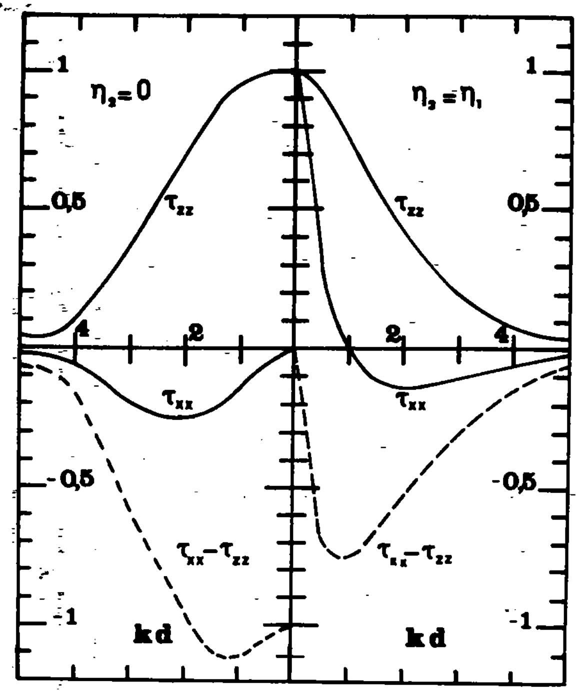

Fig. A2. Plot of the surface stresses versus wavenumber computed for the simple structure depicted in Figure A1. On the left the lower layer has zero viscosity. On the right its viscosity is the same as for the top layer. A stress value equal to unity corresponds to the weight of the deep seated mass anomaly.

$$u = \frac{\partial mgd}{2\eta} \frac{\cosh(kd)}{kd + \sinh(kd)\cosh(kd)} \sin(kx) \quad \text{(B13)}$$

$$\tau_{zz} = \partial mg \frac{kd\cosh(kd) + \sinh(kd)}{kd + \sinh(kd)\cosh(kd)} \cos(kx) \quad \text{(B14)}$$

$$\tau_{xx} = \partial mg \frac{\sinh(kd) - kd\cosh(kd)}{kd + \sinh(kd)\cosh(kd)} \cos(kx) \quad \text{(B15)}$$

These quantities are plotted on the lefthand side of the Figure A2. The main difference from the half-space solution is that τ_{xx} vanishes at large wavelength. This means that, at large wavelength, the deformation is no more inhibited by viscous flow in layer 2.

Case III : Viscous Half-space or Plate Overlain by an Elastic Lid

The upper part of the Earth's lithosphere being able to sustain stresses, an elastic lid has been added to the simple models presented above (Figure A3). This only changes the boundary condition at the top of layer 1 as free slip is replaced by no slip. Instead of equation (B2) one has now for a vanishing surface horizontal velocity :

$$A_1 + B_1 - C_1 + D_1 = 0 \quad \text{(B16)}$$

Combining this with (B1) and (B3) to (B7) one finds again the appropriate integration constants for both the half-space model ($\eta_1 = \eta_2$) and the plate model ($\eta_2 = 0$). This yields for z = 0

$$\tau_{zz} = \partial mg(1 + kd)\, e^{-kd} \cos(kx) \qquad \text{(half-space)} \quad \text{(B17)}$$

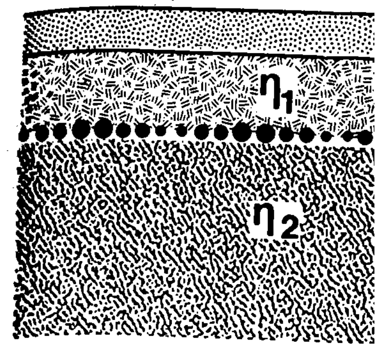

Fig. A3. Similar to Figure A

$$\tau_{zz} = \partial mg \frac{\cosh(kd) + kd\sinh}{\cosh^2(kd) + (kd)^2}$$

Figure A4 depicts this quan of the topography multiplied b ity of the elastic lid. As the τ_{zz} at the top of the fluid la neath the lid is now finite :

$$\tau_{xz} = \partial mgkd\, e^{-kd} \sin(kx)$$

$$\tau_{xz} = \partial mgkd \frac{\cosh(kd)}{\cosh^2(kd) + (kd)^2}$$

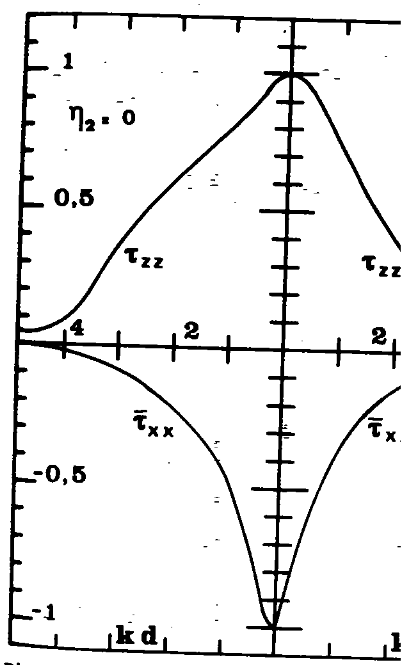

Fig. A4. Plot of the vertical s and of the horizontal averaged s number for the structure depicte the same as in Figure A2. For τ_{xx} the weight of the deep seated ma

number computed for
left the lower layer
the same as for the
ds to the weight of

(B13)

(B14)

(B15)

de of the Figure A2.
s that τ_{xx} vanishes at
ngth, the deformation

an Elastic Lid

able to sustain stres-
odels presented above
ion at the top of layer
equation (B2) one has

(B16)

inds again the appro-
e model ($\eta_1 = \eta_2$) and

(B17)

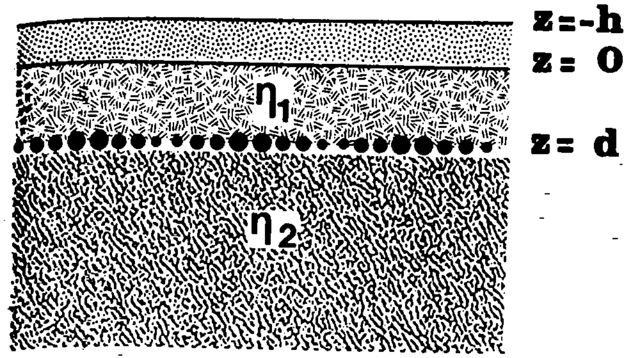

Fig. A3. Similar to Figure A1 but with an elastic lid of thickness h.

$$\tau_{zz} = \partial mg \; \frac{\cosh(kd) + kd \sinh(kd)}{\cosh^2(kd) + (kd)^2} \cos(kx) \quad \text{(plate)} \tag{B18}$$

Figure A4 depicts this quantity which is equivalent to the amplitude of the topography multiplied by $\rho g(1 + Dk^4)$ where D is the flexural rigidity of the elastic lid. As the surface velocity is zero τ_{xx} is equal to τ_{zz} at the top of the fluid layer. However the shear stress τ_{xz} underneath the lid is now finite :

$$\tau_{xz} = \partial mgkd \; e^{-kd} \sin(kx) \quad \text{(half-space)} \tag{B19}$$

$$\tau_{xz} = \partial mgkd \; \frac{\cosh(kd)}{\cosh^2(kd) + (kd)^2} \sin(kx) \quad \text{(plate)} \tag{B20}$$

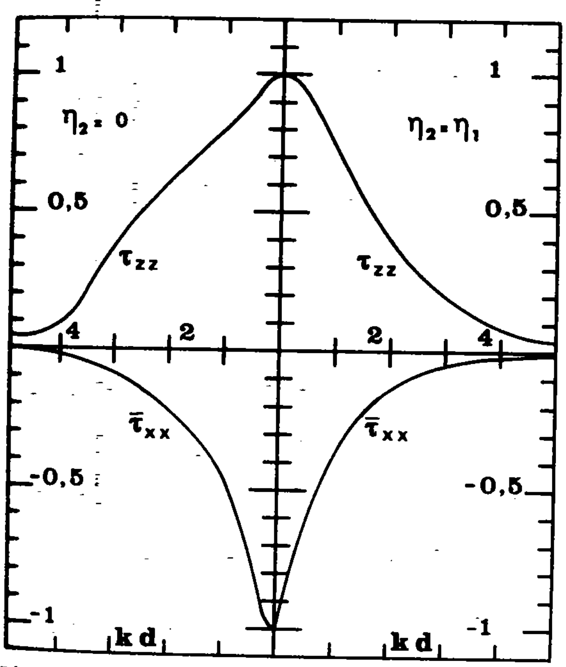

Fig. A4. Plot of the vertical stress acting underneath the elastic lid and of the horizontal averaged stress generated in the lid versus wavenumber for the structure depicted in Figure A3. The dimension for τ_{zz} is the same as in Figure A2. For τ_{xx}, however, the unit value corresponds to the weight of the deep seated mass anomaly multiplied by the ratio d/h.

This contributes to the horizontal compression or extension in the elastic lid with a vertically average value given by :

$$\bar{\tau}_{xx} = -\tau_{xz}/kh$$

(h is the thickness of the elastic lid)

Thus :

$$\bar{\tau}_{xx} = \frac{\partial mgd}{h} e^{-kd} \cos(kx) \qquad \text{(lid over half-space)} \qquad \text{(B21)}$$

$$\bar{\tau}_{xx} = \frac{\partial mgd}{h} \frac{\cosh(kd)}{\cosh^2(kd) + (kd)^2} \cos(kx) \qquad \text{(lid over space)} \qquad \text{(B22)}$$

At large wavelengths the amplitudes of the mean horizontal stress $\bar{\tau}_{xx}$ due to the shear stress τ_{xz} underneath the lid is equal to $- \partial mgd/h$, showing that the deeper the mass fluctuation the larger the stresses in the lid. This only holds for $kd < 1$.

For a deflected lid the quantities given in formula (B21) and (B22) still represent the mean non hydrostatic stress in the lid. The dynamic role of the basal shear stress τ_{xz} on the plate movements has been investigated by similar methods [Hager and O'Connell, 1981]. Moreover, this basal shear stress has been invoked for explaining local variations in the crustal stress pattern [McGarr, 1982].

APPENDIX 3 : CHANGING THE VISCOSITY CONTRAST IN THE FIVE LAYER MODEL

The standard five-layer model of Figure 1 has the following viscosity values starting with that of the top layer : $10\eta_o$, $10\eta_o$, $10\eta_o$, η_o, $\eta_o/100$. Two more sets of values have been used. The first assumes a softer lower lithosphere with $10\eta_o$, $10\eta_o$, $10\eta_o$, $\eta_o/10$, $\eta_o/1000$. The second, on the contrary, increases the asthenospheric viscosity with $10\eta_o$, $10\eta_o$, $10\eta_o$ η_o, η_o. Figure A5 gives the solutions for the standard model already found in Figure 2 as well as the new solutions.

For $k \geqslant 1$ the variations are hardly noticeable. When k approaches zero the surface value of τ_{xx} differs markedly in the two new cases.

For softer lower layers than in the standard model τ_{xx} has become larger. Equation 7 accounts for this effect : the softer lower lithosphere implies a larger value of $\eta/\bar{\eta}$ at the surface. In the case of a reduced viscosity contrast for the asthenosphere τ_{xx} is seen to shoot up towards τ_{zz}. Such a behavior was already noticed in appendix 2 for the case of a homogeneous viscous half-space. In fact this behavior of τ_{xx} is numerically present in all models but for values of k so close to zero that it cannot show on the graphs. Therefore it usually corresponds to such large wavelengths that it remains outside of the field of geophysical applications.

APPENDIX 4 : THE THREE DIMENSIONAL MATHEMATICAL TREATMENT

Let us again assume a structure with mechanical properties varying only vertically, and consisting of horizontal layers having a uniform Newtonian viscosity and let us generalize to three dimensions the formulation found in appendix 1. Using a similar notation one introduces a density distribution $\Delta\rho = \partial\rho \cos(\alpha x) \cos(\beta y)$, where x and y are the two horizontal axes. The horizontal velocities u and v, the vertical velocity w and the non hydrostatic pressure can be written

$$u = h(z) \sin(\alpha x) \cos(\beta y) \qquad \text{(D1)}$$

$$v = i(z) \cos(\alpha x) \sin(\beta y) \qquad \text{(D2)}$$

$$w = j(z) \cos(\alpha x) \cos(\beta y) \qquad \text{(D3)}$$

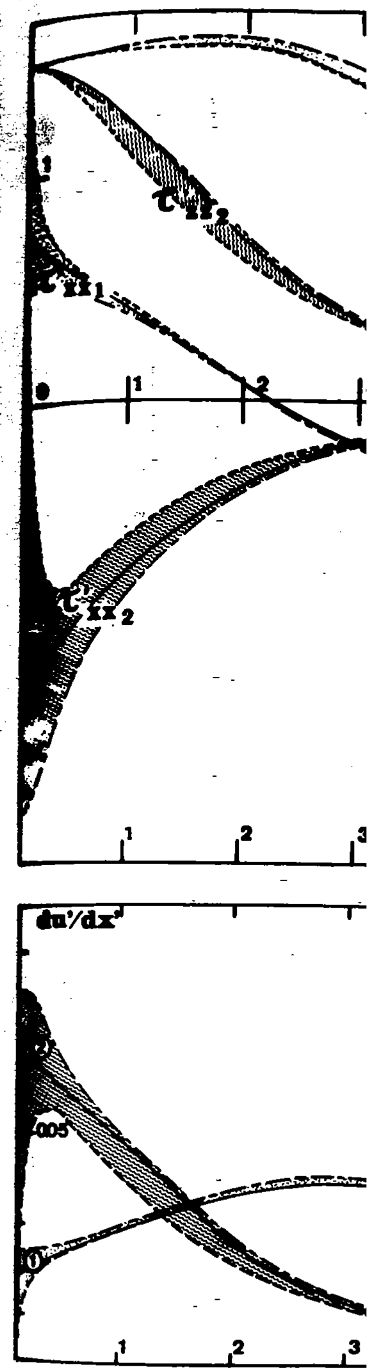

Fig. A5. Similar to Figure 2
the standard viscosity distri
Two additional solutions are
varying the viscosity distrib
similar five layer structure,
of layer 4, (η_o). The other c
contrary for a lower viscosi

sion or extension in the
;iven by :

alf-space) (B21)

ver space) (B22)

ıe mean horizontal stress $\bar{\tau}_{xx}$
ld is equal to $-\partial mgd/h$,
the larger the stresses in

in formula (B21) and (B22)
ess in the lid. The dynamic
ate movements has been inves-
ell, 1981]. Moreover, this
aining local variations in

IN THE FIVE LAYER MODEL

has the following viscosity
$10\eta_o$, $10\eta_o$, $10\eta_o$, η_o, $\eta_o/100$.
first assumes a softer lower
1000. The second, on the
sity with $10\eta_o$, $10\eta_o$, $10\eta_o$
e standard model already
ns.
eable. When k approaches zero
the two new cases.
dard model τ_{xx} has become
: the softer lower litho-
surface. In the case of a
here τ_{xx} is seen to shoot
noticed in appendix 2 for
. In fact this behavior of
for values of k so close to
efore it usually corresponds
tside of the field of geo-

CAL TREATMENT

anical properties varying
l layers having a uniform
three dimensions the formu-
notation one introduces a
, where x and y are the two
and v, the vertical velocity
itten

(D1)
(D2)
(D3)

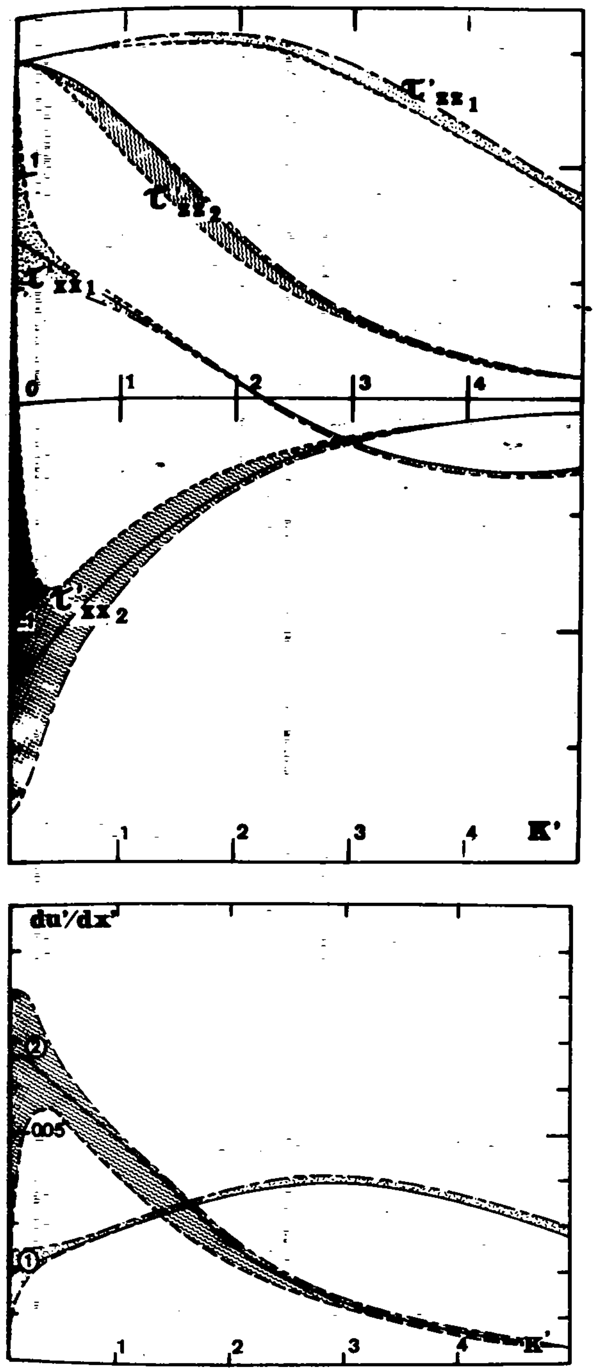

Fig. A5. Similar to Figure 2. The full line repeats the solutions for the standard viscosity distribution in the five layer model of Figure 1. Two additional solutions are plotted here in order to test the effect of varying the viscosity distribution. The dashed curves correspond to a similar five layer structure, but layer 5 has a viscosity as high as that of layer 4, (η_o). The other curves (long and short dashes) are on the contrary for a lower viscosity in layers 4 and 5 ($\eta_o/10$ and $\eta_o/100$).

$$P = p(z)\cos(\alpha x)\cos(\beta y) \tag{D4}$$

The continuity and Navier-Stokes equations yield :

$$\alpha h + \beta i + \frac{dj}{dz} = 0 \tag{D5}$$

$$\alpha p + \eta\left(-k^2 h + \frac{d^2h}{dz^2}\right) = 0 \tag{D6}$$

$$\beta p + \eta\left(-k^2 i + \frac{d^2i}{dz^2}\right) = 0 \tag{D7}$$

$$-\frac{dp}{dz} + \eta\left(-k^2 j + \frac{d^2j}{dz^2}\right) = -\partial\rho g \tag{D8}$$

Where $k^2 = \alpha^2 + \beta^2$. Again these equations can be combined to form a fourth order differential equation involving only the unknown functional $j(z)$ and identical to (A.10).

$$\frac{d^4j}{dz^4} - 2k^2\frac{d^2j}{dz^2} + k^4 j - \frac{k^2\partial\rho g}{\eta} = 0 \tag{D9}$$

The solutions are now

$$j(z) = (A + Bkz)\,e^{kz} + (C + Dkz)\,e^{-kz} + \frac{\partial\rho g}{\eta k^2} \tag{D10}$$

$$h(z) = \frac{\alpha}{k}\left[-(A + B + Bkz)\,e^{kz} + (C - D + Dkz)\,e^{-kz}\right] \tag{D11}$$

$$i(z) = \frac{\beta}{k}\left[-(A + B + Bkz)\,e^{kz} + (C - D + Dkz)\,e^{-kz}\right] \tag{D12}$$

$$p(z) = 2\eta k\,(Be^{kz} + De^{-kz}) \tag{D13}$$

The corresponding expressions for the stresses are

$$\tau_{xx} = 2\eta\left\{\frac{\alpha^2}{k}\left[-(A + B + Bkz)\,e^{kz} + (C - D + Dkz)\,e^{-kz}\right] - k(Be^{kz} + De^{-kz})\right\}\cos(\alpha x)\cos(\beta y) \tag{D14}$$

$$\tau_{yy} = 2\eta\left\{\frac{\beta^2}{k}\left[-(A + B + Bkz)\,e^{kz} + (C - D + Dkz)\,e^{-kz}\right] - k(Be^{kz} + De^{-kz})\right\}\cos(\alpha x)\cos(\beta y) \tag{D15}$$

$$\tau_{zz} = 2\eta k\left[(A + Bkz)\,e^{kz} - (C + Dkz)\,e^{-kz}\right]\cos(\alpha x)\cos(\beta y) \tag{D16}$$

$$\tau_{xy} = 2\eta\frac{\alpha\beta}{k}\left[(A + B + Bkz)\,e^{kz} - (C - D + Dkz)\,e^{-kz}\right]\sin(\alpha x)\sin(\beta y) \tag{D17}$$

$$\tau_{xz} = -2\eta\alpha\left[(A + B + Bkz)\,e^{kz} + (C - D + Dkz)\,e^{-kz} + \frac{\partial\rho g}{\eta k^2}\right]\sin(\alpha x)\cos(\beta y) \tag{D18}$$

$$\tau_{yz} = -2\eta\beta\left[(A + B + Bkz)\,e^{kz} + (C - D + Dkz)\,e^{-kz} + \frac{\partial\rho g}{\eta k^2}\right]\cos(\alpha x)\sin(\beta y) \tag{D19}$$

For $\beta = 0$ these solutions are identical to the two dimensional solutions of appendix 1. The relative amplitudes of the velocities u and v are in the ratio α/β. For the deformations $\partial u/\partial x$ and $\partial v/\partial y$ this rato is α^2/β^2.

The deformation of the struc
the shortest wavelength, i.e.

APPENDIX 5 : SOLUTIONS FOR A
MECHANICAL PROPE

In a thin layer overlying
concentric regions of viscosi
bounded by a circle of radius
a circle of radius r_2 to infi
the inner region. According t
gion as being a plateau that
shrinking because of its cold
and angular coodinate in the
tion.

In the radial direction th
horizontal stresses :

$$\frac{d\tau_r}{dr} + \frac{1}{r}(\tau_r - \tau_\phi) = 0$$

On the other hand the constitu
plane yields two equations inv
mal stresses :

$$\frac{2}{3}\tau_r - \frac{1}{3}\tau_\phi - \frac{1}{3}\tau_z = 2\eta \ldots$$

$$\frac{2}{3}\tau_\phi - \frac{1}{3}\tau_r - \frac{1}{3}\tau_z = 2\eta \ldots$$

Remember that τ_z is equal to –
were. Combining (E1), (E2) and
derives a second order differe

$$\frac{d^2V_r}{dr^2} + \frac{1}{r}\frac{dV_r}{dr} - \frac{V_r}{r^2} = 0$$

This has the general solution :

$$V_r = Ar + \frac{B}{r}$$

Where A and B are integration c
The stresses are obtained from

$$\tau_r = \tau_z + 2\eta\left(2\frac{dV_r}{dr} + \frac{V_r}{r}\right) = \tau_z + \ldots$$

$$\tau_\phi = \tau_r + 2\eta\left(\frac{V_r}{r} - \frac{dV_r}{dr}\right) = \tau_z + 6\ldots$$

Notice that a solution of the ty
ning or thickening of the lithos
other hand, a solution of the ty
slip with $\tau_r = \tau_z - 2\eta B/r^2$ and τ

Considering now the three conc
(E5) for each region using appro
dary conditions will help to det

The deformation of the structure is thus the largest in the direction of the shortest wavelength, i.e. of the shortest axis of the structure.

APPENDIX 5 : SOLUTIONS FOR A LAYER WITH RADIAL VARIATIONS OF THE MECHANICAL PROPERTIES

In a thin layer overlying an inviscid fluid let us consider three concentric regions of viscosities η_1, η_2, and η_3. The inner region is bounded by a circle of radius r_1, whereas the outer region extends from a circle of radius r_2 to infinity. A mass anomaly Δm sits at the base of the inner region. According to its sign one may think of the central region as being a plateau that tends to spread out ($\Delta m < 0$) or an area shrinking because of its cold root ($\Delta m > 0$). Let r and ϕ be the radial and angular coodinate in the horizontal plane and z the vertical direction.

In the radial direction the equilibrium yields a relationship between horizontal stresses :

$$\frac{d\tau_r}{dr} + \frac{1}{r}(\tau_r - \tau_\phi) = 0 \qquad \text{(E1)}$$

On the other hand the constitutive viscous relationship in the horizontal plane yields two equations involving the radial velocity V_r and the normal stresses :

$$\frac{2}{3}\tau_r - \frac{1}{3}\tau_\phi - \frac{1}{3}\tau_z = 2\eta\frac{dV_r}{dr} \qquad \text{(E2)}$$

$$\frac{2}{3}\tau_\phi - \frac{1}{3}\tau_r - \frac{1}{3}\tau_z = 2\eta\frac{V_r}{r} \qquad \text{(E3)}$$

Remember that τ_z is equal to $-\Delta mg$ beneath the plateau and vanishes elsewere. Combining (E1), (E2) and (E3) in order to eliminate τ_r and τ_ϕ, one derives a second order differential equation involving only V_r :

$$\frac{d^2V_r}{dr^2} + \frac{1}{r}\frac{dV_r}{dr} - \frac{V_r}{r^2} = 0 \qquad \text{(E4)}$$

This has the general solution :

$$V_r = Ar + \frac{B}{r} \qquad \text{(E5)}$$

Where A and B are integration constants.
The stresses are obtained from expression derived from (E2) and (E3) :

$$\tau_r = \tau_z + 2\eta\left(2\frac{dV_r}{dr} + \frac{V_r}{r}\right) = \tau_z + 2\eta\left(3A - \frac{B}{r^2}\right) \qquad \text{(E6)}$$

$$\tau_\phi = \tau_r + 2\eta\left(\frac{V_r}{r} - \frac{dV_r}{dr}\right) = \tau_z + 6\eta A + 2\eta\frac{B}{r^2} \qquad \text{(E7)}$$

Notice that a solution of the type $V_r = Ar$ corresponds to uniform thinning or thickening of the lithosphere with $\tau_\phi = \tau_r$ everywhere. On the other hand, a solution of the type $V_r = B/r$ corresponds to pure strike slip with $\tau_r = \tau_z - 2\eta B/r^2$ and $\tau_\phi = \tau_z + (2\eta B/r^2)$.

Considering now the three concentric regions one writes the solution (E5) for each region using appropriate indices 1, 2, or 3. Various boundary conditions will help to determine the values of the six integration constants. To avoid diverging velocities and stresses in region 1, B_1 must be zero. At the interface of two layers the radial velocity V_r and stress τ_r must be continuous. It implies :

$$A_1 r_1 = A_2 r_1 + \frac{B_2}{r_1} \qquad \text{(E8)}$$

$$A_3 r_2 + \frac{B_3}{r_2} = A_2 r_2 + \frac{B_2}{r_2} \qquad \text{(E9)}$$

$$3\eta_1 A_1 + \frac{\tau_z}{2} = \eta_2 \left(3A_2 - \frac{B_2}{r_1^2}\right) \qquad \text{(E10)}$$

$$\eta_3 \left(3A_3 - \frac{B_3}{r_2^2}\right) = \eta_2 \left(3A_2 - \frac{B_2}{r_2^2}\right) \qquad \text{(E11)}$$

The conditions at large distances determine one last relationship. For a vanishing stress, A_3 has to be zero. Let us calculate the solutions for this particular case. They are

$$A_1 = \frac{\tau_z}{2\mu} \left[(\eta_3 - \eta_2) - \frac{r_2^2}{r_1^2}(3\eta_2 + \eta_3)\right] \qquad \text{(E12)}$$

$$A_2 = \frac{\tau_z}{2\mu}(\eta_3 - \eta_2) \qquad \text{(E13)}$$

$$B_2 = -\frac{\tau_z}{2\mu} r_2^2 (3\eta_2 + \eta_3) \qquad \text{(E14)}$$

$$B_3 = -\frac{\tau_z}{2\mu} 4\eta_2 r_2^2 \qquad \text{(E15)}$$

where $\mu = (r_2^2/r_1^2)(3\eta_1 + \eta_2)(3\eta_2 + \eta_3) + (\eta_1 - \eta_2)(\eta_2 - \eta_3)$ is always positive. Thus some properties of this physical solution can be discussed. In the central region A has a sign opposite to Δm. This implies that whatever the surounding viscosity this region is in extension for $\Delta m < 0$ and in compression for $\Delta m > 0$.

In the intermediate region A has the sign of $\Delta m(\eta_3 - \eta_2)$. This region will experience pure strike slip if its viscosity is equal to that of the outer zone ($\eta_2 = \eta_3$), extension if $\Delta m(\eta_3 - \eta_2) > 0$ and compression if $\Delta m(\eta_3 - \eta_2) < 0$. This means that its tectonic regime is critically determined both by the rheogogical properties and by the density heterogeneities in the neighbouring areas. This point is the major novelty deriving from this quasi three dimensional treatment.

In contrast with the above conclusion let us remark that for a uniform viscosity ($\eta_1 = \eta_2 = \eta_3$) the local thinning or thickening rate only depends upon the local value of Δm. Indeed (A7) shows that (A2) vanishes so that no thickening occurs outside the central region. In this last region, equation (E12) shows that the thickening rate $[-(\partial V_r/\partial_r) - V_r/r]$ is equal to $-(\partial mg/4\eta)$. Two dimensional models lead exactly to the same result.

The case of a non-vanishing stress at infinity remains to be considered. More precisely one wants to solve the system (E8) to (E11) for the case $\Delta m = 0$ but $A_3 = (\tau_\infty/6\eta_3)$ (see E6 and E7).

$$A_1 = \frac{2}{3}\tau_\infty \left[1 + 3\left(\frac{\eta_2}{\eta_1} - 1\right) \Big/ \left(3 + \frac{\eta_2}{\eta_1}\right)\right] \Big/ \nu \qquad \text{(E16)}$$

$$A_2 = \frac{2}{3}\tau_\infty / \nu \qquad \text{(E17)}$$

$B_2 = 2\tau_\infty \left(\frac{\eta_2}{\eta_1} - 1\right) / \left(3 + \frac{\eta_2}{\eta_1}\right.$

$B_3 = (A_2 - A_3)\, r_2^2 + B_2$

with $\nu = (\eta_3 + 3\eta_2) - \frac{r_1^2}{r_2^2}$ [3(

One specific application c
τ_∞ capable of sustaining the
corresponding topography in
one requires $\tau_z = \tau_\phi = \tau_r$ fo
for the case where the intern
viscosity ($\eta_1 = \eta_2$). It read

$\tau_\infty = \frac{3}{16}\Delta mg \left[\left(3 + \frac{\eta_3}{\eta_1}\right) + \frac{r_1^2}{r_2^2}\right.$

This far-field stress is
the viscosities. This is jus
the presence of lateral chan
deformation in one area depe

Acknowledgments. During t
with geologists and geophysi
were of great benefit to us.
Tuen have helped improving t

REFERENCES

Artyushkov, E. V., The stres
thickness inhomogeneities,
Artyushkov, E. V., Can the E
J. Geophys. Res., 79, 741-
Baer, M., Relative travel time
Suiss seismic station netw
Bird, P., and J. Baumgardner
J. Geophys. Res., 86, 4891-
Cathles, L. M., III, The visc
University Press, Princeto
Dalmayrac, B. and P. Molnar,
and constraints on the sta
473-481, 1981.
Frank, F. C., Plate tectonics
in Flow and Fracture of Roc
I.Y. Borg, N.L. Carter and
Geophys. Monogr., 1972.
Frechet, J., Sismicité du Su
de zonage sismique, Thèse
Froidevaux, C., C. Paquin and
in situ measurements with a
1980.
Hager, B. H. and R. J. O'Conn
and Mantle convection, J. G
Houseman, G. A., D. P. Mc Kenz
a thickened boundary layer
of continental convergent b
Hovland, J., D. Gubbins and E
beneath Central Europe, Ge
Isacks, B. and P. Molnar, Dis

tresses in region 1, B_1
ie radial velocity V_r and

(E8)

(E9)

(E10)

(E11)

ne last relationship. For
alculate the solutions

(E12)

(E13)

(E14)

(E15)

$\eta_2)$ $(\eta_2 - \eta_3)$ is always
solution can be discussed.
Δm. This implies that wha-
n extension for $\Delta m < 0$ and

$\Delta m(\eta_3 - \eta_2)$. This region
ty is equal to that of
$\eta_2) > 0$ and compression
c regime is critically
nd by the density hetero-
is the major novelty
tment.
remark that for a uni-
g or thickening rate only
shows that (A2) vanishes
l region. In this last
g rate $[-(\partial V_r/\partial_r) - V_r/r]$
ead exactly to the same

remains to be considered.
3) to (E11) for the case

(E16)

(E17)

$$B_2 = 2\tau_\infty \left(\frac{\eta_2}{\eta_1} - 1\right) / \left(3 + \frac{\eta_2}{\eta_1}\right) r_1^2 / \nu \qquad \text{(E18)}$$

$$B_3 = (A_2 - A_3)\, r_2^2 + B_2 \qquad \text{(E19)}$$

$$\text{with } \nu = (\eta_3 + 3\eta_2) - \frac{r_1^2}{r_2^2}\,[3(\eta_1 - \eta_2)\,(\eta_3 - \eta_2) / (3\eta_1 + \eta_2)].$$

One specific application consists in computing the far field stress τ_∞ capable of sustaining the central region with its density anomaly and corresponding topography in a state of vanishing deformation. For this one requires $\tau_z = \tau_\phi = \tau_r$ for $r < r_1$. For simplicity we give the answer for the case where the intermediate and central regions have the same viscosity $(\eta_1 = \eta_2)$. It reads

$$\tau_\infty = \frac{3}{16}\,\Delta mg \left[\left(3 + \frac{\eta_3}{\eta_1}\right) + \frac{r_1^2}{r_2^2}\left(1 - \frac{\eta_3}{\eta_1}\right)\right] \qquad \text{(E20)}$$

This far-field stress is thus dependent upon the relative value of the viscosities. This is just another illustration of the fact that in the presence of lateral changes in mechanical properties stresses and deformation in one area depend upon the strength of neighbouring regions.

Acknowledgments. During the initial stage of this work, discussions with geologists and geophyisicists, in particular with Paul Tapponnier, were of great benefit to us. Constructive remarks by Peter Bird and David Yuen have helped improving the final version of this paper.

REFERENCES

Artyushkov, E. V., The stresses in the lithosphere caused by crustal thickness inhomogeneities, J. Geophys. Res., 78, 7675-7708, 1973.
Artyushkov, E. V., Can the Earth's crust be in a state of isostasy ? J. Geophys. Res., 79, 741-752, 1974.
Baer, M., Relative travel time residuals for tele seismic events at the new Swiss seismic station network, Annales de Géophysique, 36, 119-126, 1980.
Bird, P., and J. Baumgardner, Steady propagation of delamination events, J. Geophys. Res., 86, 4891-4903, 1981.
Cathles, L. M., III, The viscosity of the Earth's Mantle, Princeton University Press, Princeton, N.J. 1975.
Dalmayrac, B. and P. Molnar, Parallel thrust and normal faulting in Peru and constraints on the state of stress, Earth Planet. Sci. Lett., 55, 473-481, 1981.
Frank, F. C., Plate tectonics, the analogy with glacier flow and isostasy, in Flow and Fracture of Rocks, the Griggs Volume, edited by H.C. Heard I.Y. Borg, N.L. Carter and C.B. Raleigh, pp 285-292, Am. Geophys. Union, Geophys. Monogr., 1972.
Frechet, J., Sismicité du Sud-Est de la France, et une nouvelle méthode de zonage sismique, Thèse 3ème cycle, Univ. sc. Medic. Grenoble, 1978.
Froidevaux, C., C. Paquin and M. Souriau, Tectonic stresses in France : in situ measurements with a flat jack, J. Geophys. Res., 85, 6342-6346, 1980.
Hager, B. H. and R. J. O'Connell, A simple global model of plate dynamics and Mantle convection, J. Geophys. Res., 86, 4843-4867, 1981.
Houseman, G. A., D. P. Mc Kenzie and P. Molnar, Convective instability of a thickened boundary layer and its relevance for the thermal evolution of continental convergent belts, J. Geophys. Res., 86, 6115-6132, 1981.
Hovland, J., D. Gubbins and E. S. Husebye Upper Mantle heterogeneities beneath Central Europe, Geophys. J.R. Astron. Soc., 66, 261-264, 1981.
Isacks, B. and P. Molnar, Distribution of stresses in the descending

lithosphere from a global survey of focal mechanism solutions of Mantle earthquakes, Rev. Geophys. Space Phys., 9, 103-174, 1971.
Le Pichon, X. and J. Angelier, The Hellenic arc and trench system : A key to the neotectonic evolution of the eastern mediterranean area, Tectonophysics, 60, 1-42, 1979.
Lliboutry, L. A., Isostasie, propriétés rhéologiques du manteau supérieur, in Traité de Géophysique interne, edited by J. Coulomb and G. Jobert, pp 473-505, Masson et Cie, 1973.
Mc Garr, A., Analysis of state of stress between provinces of constant stress, submitted to J. Geophys. Res., 1982.
Mc Kenzie, D. P., Active tectonics of the Alpine Himalayan belt : The aegean sea and surrounding regions, Geophys. J. R. Astron Soc., 55, 217-254, 1978.
Mc Nutt, M., Implications of regional gravity for state of stress in the Earth's crust and upper Mantle, J. Geophys. Res., 85, 6377-6396, 1980.
Mercier, J. L., Extensional-compressional tectonics associated with the Aegean arc. Comparison with the Andean Cordillera of South Peru North Bolivia, Philos. Trans. R. Soc. London, A 300, 337-355, 1981.
Molnar, P. and P. Tapponnier, A possible dependence of tectonic strength on the age of the crust in Asia, Earth Planet. Sci. Lett., 52, 107-114, 1981.
Nataf, H. C., C. Froidevaux, J. L. Levrat, and M. Rabinowicz, Laboratory convection experiments ; effect of lateral cooling and generation of instabilities in the horizontal boundary layers, J. Geophys. Res., 86, 6143-6154, 1981.
Panza, G. F. and S. Mueller, The plate boundary between Eurasia and Africa in the Alpine area, Mem. Sc. Geol., 33, 43-50, 1979.
Paquin, C., C. Froidevaux, J. Bloyet, Y. Ricard, and C. Angelidis, Tectonic stresses on the mainland of Greece ; in situ measurements by overcoring, submitted to Tectonophysics, 1982.
Pavoni, N., Erdbeben in Gebiet der Schweiz Ecologae Geol. Helv, 70, 751-370, 1977.
Philip, H., Tectonique récente et sismicité de la France : caractéristiques géodynamiques - Géologie de la France, 26ème C.G.I. Mémoire B.R.G.M., 107, 42-46, 1980.
Poupinet, G., Sur l'existence d'un manteau à très faible vitesse sous les Alpes occidentales et ses implications tectoniques, Bull. Soc. Geol. Fr., 27, 1073-1083, 1976.
Richardson, R. M., S. C. Solomon, and N. H. Sleep, Tectonic stress in the plates, Rev. Geophys. Space Phys., 17, 981-1019, 1979.
Sprecher, Ch., 1976. Die Struktur des oberen Erdmantels in Zentraleuropa aus Dispersinmessungen an Rayleigh-Wellen, Ph. D. Thesis, Eidg. Tech. Hochsch. Zürich, 156 pp.
Takeuchi, H. and Y. Hasegawa Viscosity distribution within the Earth, Geophys. J., 9, 503-508, 1965.
Tapponnier, P., and P. Molnar, Slip line field theory and large scale continental tectonics, Nature, 264, 319-324, 1976.
Tapponnier, P., Evolution tectonique du système alpin en Mediterranée, poinçonnement et écrasement rigide-plastique, Bull. Soc. Geol. Fr., 19, 437-460, 1977.
Werner, D., and E. Kissling, Geothermics and gravity within the Swiss Alps, Terra cognita, 0, 77, 1981.
Yuen, D. A., W. R. Peltier, and G. Schubert, On the existence of a second scale of convection in the upper Mantle, Geophys. J. R. Astron. Soc, 65, 171-190, 1981.
Zoback, M. L., and M. Zoback, State of stress in the conterminous United States, J. Geophys. Res., 85, 6113-6156, 1980.

(Received November 2, 1981 ;
accepted November 16, 1981)

STRAIN, STRESS AND UPLIFT

Mitsuhiro Toriumi

Department of Earth Scienc
Bunko-cho 2-5, Matsuyama,

Abstract. Strain distr
Sambagawa regional metamor
change of initially spheri
2000% with increasing meta
increase apparently occurs
the terrane. Deformation
using the grain-sized quar
to dynamically recrystalli
across the terrane was co
the lower-grade zones was
was about 50 MPa. Combini
and temperatures of the st
energy of the deformation
have been about 80-90 kJ/m
deep-seated Sambagawa meta
at the lower crustal to upp
lithosphere, was sufficient
terrane to the earth's sur

INTRODUCTION

High pressure metamorphi
around subduction and colli
Bird, 1970]. The process o
is partly revealed in recen
glaucophanitic Sabagawan an
al., 1970; Ernst, 1975; Cow
al., 1978; Otsuki, 1980].
increased with pressure in
dropped at relative constan
Petrological evidence sugge
elevation are very rapid co
ature homogenization of the
Large-scale recumbent fo
been recognized in the high
Ernst et al. [1970] and Kur
trative deformation of rock
lower-grade zones were not
weak foliation and open fol
is composed of many thrust
et al., 1977]. Therefore t
to increase with increasing
determined by shape change
laria in cherty rocks of the
formed pebbles in the congl

Paper number 1T1782. 0278-7